Appl. Magn. Reson. 4, 1–64 (1993)

**Applied Magnetic Resonance**



# Application of $^{27}$Al NMR Techniques to Structure Determination in Solids

**M.E. Smith**

CSIRO Division of Materials Science and Technology, Clayton, Victoria, Australia

Received November 19, 1991; revised December 8, 1991

**Abstract.** There have been great improvements in the quality of $^{27}$Al NMR spectra from solids over the last decade. The impact of this technique on structure determination for a wide range of solids is briefly reviewed. Emphasis is placed on the effects arising from the presence of the quadrupolar interaction and strategies that allow unambiguous spectral interpretation. It is demonstrated that in addition to the chemical shift, the quadrupolar interaction itself can be a rich source of local information about solids. The insight obtained from $^{27}$Al NMR into atomic level structure often contains surprises, such that previous models of structure and properties have to be reassessed.

## 1. Introduction

Aluminium is one of the most naturally abundant elements and occurs in a wide range of solids that are of significant technological and scientific interest including minerals, zeolites, catalyst supports, ceramics, gels, glasses and thin films. To understand many of the key properties of these materials demands examination of the atomic level structure. NMR has been shown to be a powerful probe of the local structure (i.e. nearest neighbour nn and next nearest neighbour nnn) and provides complementary information to standard characterization techniques such as diffraction, microscopy and vibrational spectroscopies. $^{27}$Al is an attractive nucleus for NMR having a moderately large gyromagnetic ratio ($\gamma = 6.9763 \cdot 10^7$ rads$^{-1}$T$^{-1}$) and 100% natural abundance so that its receptivity is 20% that of $^1$H. It is a spin-5/2 ($I$) nucleus and has a moderate quadrupole moment ($eQ$) of $0.149 \cdot 10^{-28}$ m$^2$. The presence of the quadrupolar interaction can complicate interpretation of the NMR spectrum but the quadrupolar moment acts as a very sensitive probe of the electric field gradient (efg = $eq$) at the nucleus and can provide information about the local structure.

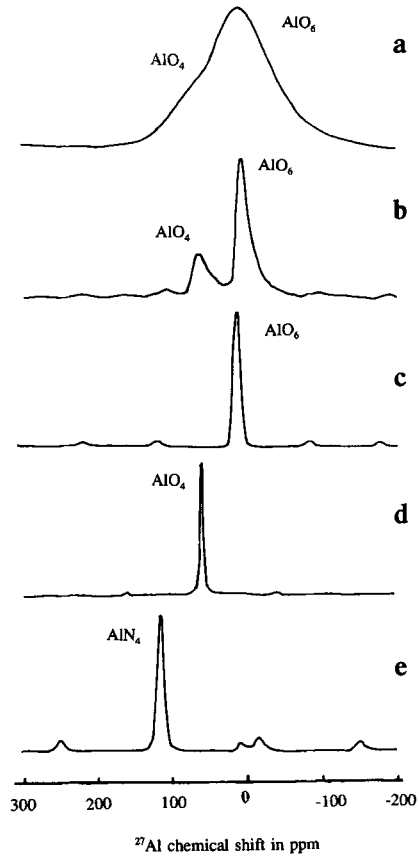


**Fig. 1.** $^{27}Al$ NMR spectra of $MgO(3.5Al_2O_3)$ spinel, **a** static and **b** MAS together with MAS spectra of **c** $\alpha$-$Al_2O_3$, **d** Na-Y zeolite and **e** AlN at 9.4 T.

In the last decade with the increasingly widespread availability of high applied magnetic fields (> 7 T) and magic angle spinning (MAS) [1] aluminium has become much studied in the solid state. $^{27}Al$ principally experiences dipolar, chemical shielding and quadrupolar interactions in diamagnetic insulating solids. An important structural question is often simply: is aluminium's local coordination tetrahedral (Al(4)), penta-coordinate (Al(5)) or octahedral (Al(6)) and to what element? NMR can usually answer this question from the value of the isotropic chemical shift ($\delta_{iso}$). For solids, application of MAS largely removes anisotropic contributions improving resolution and making identification of Al(4), Al(5) and Al(6) much more straightforward [2–6]. Fig. 1 shows the ranges of shift from some materials with well defined aluminium coordinations. The spinel $MgO \cdot (3.5Al_2O_3)$ has Al(4) and Al(6) species present and although there is some evidence for this from the static spectrum (Fig. 1a), their resolution becomes complete using MAS (Fig. 1b). The change of shift due to the nn is exemplified by comparison of zeolite

Na-Y with four oxygen nn, which resonates at 56.5 ppm (Fig. 1d), and AlN with four surrounding nitrogens (Fig. 1e) that is shifted to 114 ppm.

The ability to resolve these differences enable key questions about materials to be tackled. For example, what is the Si/Al order in framework minerals (including zeolites) and how is aluminium distributed between tetrahedral and octahedral layers in clay minerals? What structural changes occur when zeolites are dealuminated, and in glasses and ceramics as their compositions are changed? Many of these materials are poorly crystalline and/or atomically disordered so that conventional techniques, particularly diffraction can offer little insight. The impact that $^{27}$Al NMR has had in these areas is briefly reviewed. However $^{27}$Al solid state NMR did not develop at the rate of spin-1/2 nuclei such as $^{29}$Si and $^{13}$C because of a number of complications that result from the quadrupolar interaction. Structural differences that can be readily resolved as distinct spectral features from spin-1/2 nuclei are often obscured in $^{27}$Al MAS NMR spectra as a result of only partial removal of the quadrupolar broadening. Many of the early studies also reported large discrepancies between the known aluminium distribution and content compared to that deduced from NMR spectra [e.g. 7–9]. The peak position was observed to be a magnetic field dependent quantity and its usual identity with the isotropic chemical shift is invalid. As illustration, consider the polymorphs β- and γ-$LiAlO_2$ where at 6.35 T their peak positions differ by around 10 ppm, which cannot be explained on the basis of any structural influences on $\delta_{iso}$. This difference is almost entirely due to quadrupole effects (*vide infra*), which are different for the two materials (Table 4), and when suitably corrected for gives a difference in $\delta_{iso}$ of only ~ 1 ppm [10]. The following two sections are devoted to a discussion of the quadrupolar interaction and its influence on the NMR spectrum before proceeding to the applications of solid state $^{27}$Al NMR.

## 2. The Nuclear Quadrupole Interaction

Nuclei with $I > 1/2$ possess a quadrupole moment ($eQ$), resulting from a non-spherical distribution of the nuclear electric charge, which interacts with the gradient in the electric field ($\nabla\underline{\varepsilon}$) at the nucleus caused by the external charges with an energy

$$E = e\underline{Q} \cdot \nabla\underline{\varepsilon}. \tag{1}$$

This is an electrostatic interaction but the energy is determined by the $z$-component of the magnetic quantum number ($m$) thereby producing an effect on the NMR spectrum. The nuclear quadrupolar Hamiltonian may generally be written down as [11–16]

$$\mathscr{H}_Q = \frac{eQ}{4I(2I-1)}\left[\sqrt{2/3}(3I_z^2 - I(I+1))V_0 + (I_zI_+ + I_+I_z)V_{-1}\right.$$

$$\left. + (I_zI_- + I_-I_z)V_{+1} + I_+^2 V_{-2} + I_-^2 V_{+2}\right], \tag{2}$$

where $V_n$ are the components of the second-rank electric field gradient tensor. In the Principal Axes System (PAS) $V_0 = \sqrt{3/2}\,V_{ZZ} = \sqrt{3/2}\,eq$, $V_{\pm 1} = 0$ and $V_{\pm 2} = V_{XX} - V_{YY} = (eq\eta/2)$:

$$\mathscr{H}_Q^{PAS} = \frac{e^2qQ}{4I(2I-1)}\left[3I_z^2 - I(I+1) + \frac{\eta}{2}(I_+^2 - I_-^2)\right]. \tag{3}$$

Measurements are made in the laboratory frame, where the $z$-direction is defined by the applied magnetic field $B_0$ to which $\mathscr{H}_Q^{PAS}$ may be readily transformed by using the standard Wigner rotation matrices **D** [17] on the components of the efg tensor:

$$V_q^{lab} = \sum_{-2<l<2} D^{(2)}(\varphi, \vartheta, \psi)\, V_l^{PAS}, \tag{4}$$

where $(\varphi, \vartheta, \psi)$ are the Euler angles which define the orientation of the PAS in the laboratory frame. The effect $\mathscr{H}_Q$ has on the nuclear spin energy levels will be considered in the limit when the Zeeman interaction is large so that standard perturbation theory may be applied:

$$E = E_m^{(0)} + E_m^{(1)} + E_m^{(2)} + \ldots, \tag{5}$$

where

$$E_m^{(0)} = -mh\gamma B_0 \qquad \text{(Zeeman interaction)}, \tag{6}$$

$$E_m^{(1)} = \frac{eq}{4I(2I-1)}\sqrt{2/3}\,(3m^2 - I(I+1))V_0, \tag{7}$$

$$E_m^{(2)} = \left(-\frac{eQ}{4I(2I-1)}\right)^2 \frac{2}{h\nu_0}\left[V_{+1}V_{-1}(24m(m-1) - 4I(I+1) + 9)\right.$$

$$\left. + \frac{V_{-2}V_{+2}}{2}(12m(m-1) - 4I(I+1) + 6)\right]. \tag{8}$$

For static spectra the appropriate expressions for $V_n$ may simply be inserted and the effect on the frequency of a single quantum transition derived. The basic frequency will be the Larmor frequency ($\nu_0$) resulting from six equally spaced energy levels (Fig. 2a). The influence of the first-order quadrupolar perturbation is:

$$\nu_m^{(1)} = \frac{3C_q}{4I(I-1)}(3\cos^2\vartheta - 1 + \eta\sin^2\vartheta\cos 2\varphi)(m - 1/2)\,. \tag{9}$$

Practically this has two consequences, the central transition $(1/2, -1/2)$ has no first-order effects, and the non-central transitions are spread over a frequency range of order $\nu_q$ $(= 3C_q/2I(2I-1))$ which can be easily in the MHz range and hence are difficult to observe by pulsed methods (Fig. 2b). This means that usually only the central transition is observed. The quadrupolar interaction can be sufficiently large that second-order quadrupolar effects must be considered. For general $m$ and $\eta$ quite involved expressions exist (see [15]), but for the central transition these effects may be written as

$$\nu_{1/2}^{(2)} = \frac{9C_q^2}{144\nu_0}[9(3 - \eta\cos\varphi)^2\sin^4\vartheta - 12(6 + \eta^2 - 5\eta\cos 2\varphi)\sin^2\vartheta + 4\eta^2]. \tag{10}$$

This gives rise to a characteristic powder pattern (Fig. 2c) which if clearly resolved can be used to deduce $C_q$ and $\eta$, the latter clearly having a marked influence on the lineshape (Fig. 3). However the presence of other anisotropic interactions, particularly dipolar, usually smooth the lineshape obscuring the defining singularities and shoulders.

The standard technique for improving resolution and removing anisotropic contributions is to rapidly rotate the sample at the magic angle (54.7°) to the applied magnetic field. This is very effective at removing the first-order perturbations and has been discussed in much detail [18]. However the more complicated angular variation of the second-order perturbation (Eq.(10)) means that MAS at $\nu_r$ can only produce partial narrowing. Under rotation at an angle $\beta$ to the applied magnetic field the laboratory components of the efg can be written down in terms of a double angular transformation:

$$V_q^{lab} = \sum_{p=-2}^{2} D_{p,q}^{(2)}(\omega_r t, \beta, 0) \sum_{r=-2}^{2} D_{r,p}^{(2)}(\varphi, \vartheta, \psi)\, V_r^{PAS}\,. \tag{11}$$

Such transformations have been used to calculate second-order quadrupolar perturbed spectra from rotating solids [19–24]. The lineshape of the

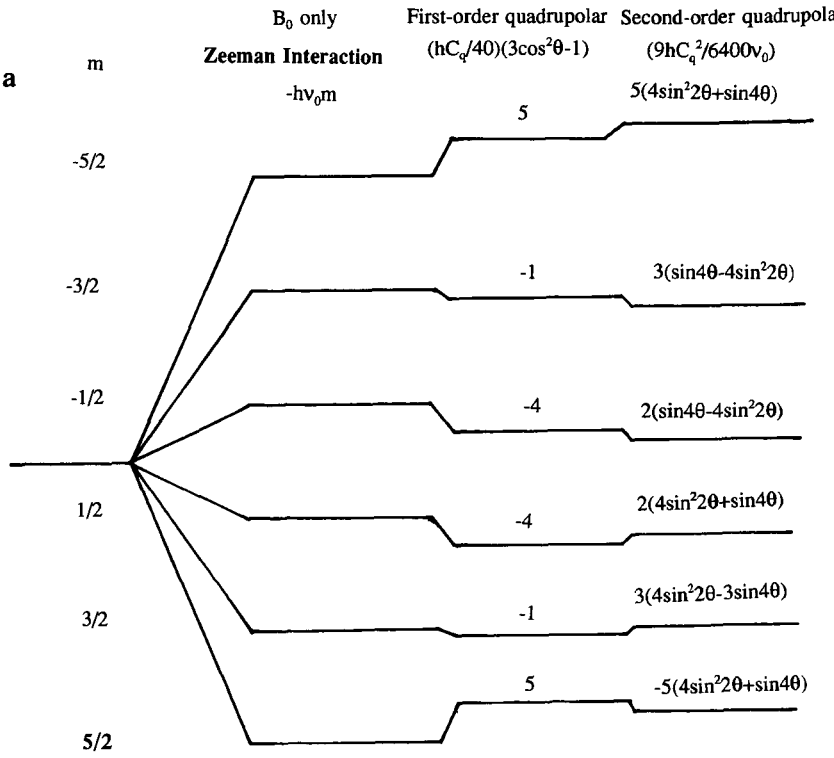
a
m
$B_0$ only
Zeeman Interaction
$-h\nu_0 m$
First-order quadrupolar
$(hC_q/40)(3\cos^2\theta-1)$
Second-order quadrupolar
$(9hC_q^2/6400\nu_0)$
$5(4\sin^2 2\theta+\sin 4\theta)$
5
-5/2
-1
$3(\sin 4\theta-4\sin^2 2\theta)$
-3/2
-4
$2(\sin 4\theta-4\sin^2 2\theta)$
-1/2
$2(4\sin^2 2\theta+\sin 4\theta)$
-4
1/2
$3(4\sin^2 2\theta-3\sin 4\theta)$
-1
3/2
5
$-5(4\sin^2 2\theta+\sin 4\theta)$
5/2

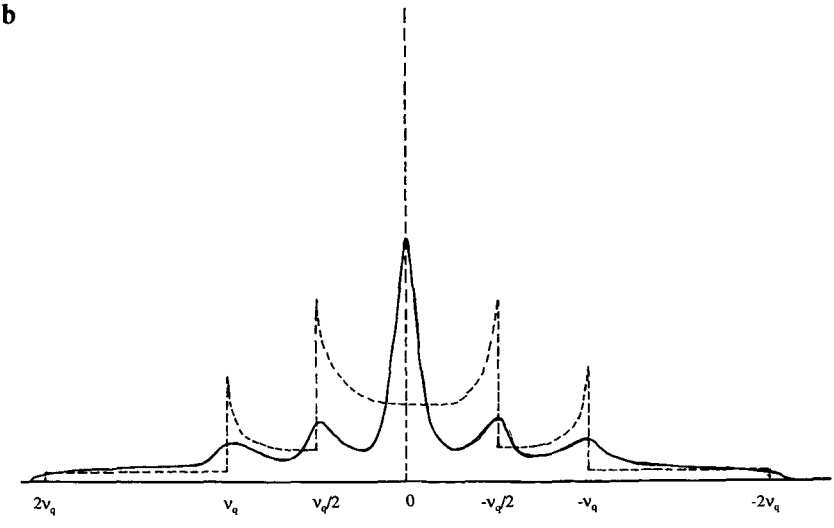
b
$2\nu_q$
$\nu_q$
$\nu_q/2$
0
$-\nu_q/2$
$-\nu_q$
$-2\nu_q$

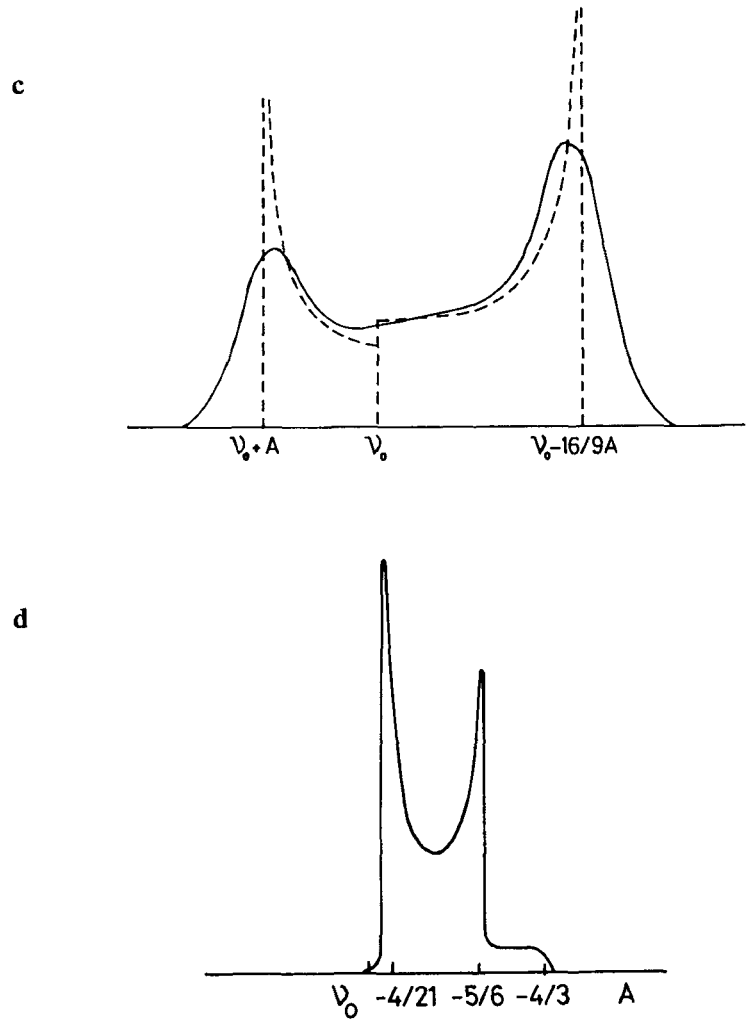


**Fig. 2.** **a** Nuclear energy levels for an $I = 5/2$ nucleus showing first and second-order quadrupolar effects and the resulting static powder patterns ($\eta = 0$) for **b** all transitions perturbed to first-order and **c** the second-order broadening of the $(1/2, -1/2)$ together with **d** its MAS spectrum. $A$ $(I(I+1) - 3/4)\nu_q/16\nu_0$.

$(m, m-1)$ transition and its related sidebands can be written down as an analytical function in the case of $\nu_r \to \infty$ which is often a good approximation for the $(1/2, -1/2)$ transition and a characteristic lineshape is still obtained (Figs. 2d and 3). For the outer transitions and when $C_q$ becomes large enough the approximation $\nu_r \sim \infty$ breaks down and a summation over different orientations of the rotor are required to obtain the lineshape [25, 26] which can be quite different from the infinite spinning speed limit and the centrebands and sidebands will in general have a different shape

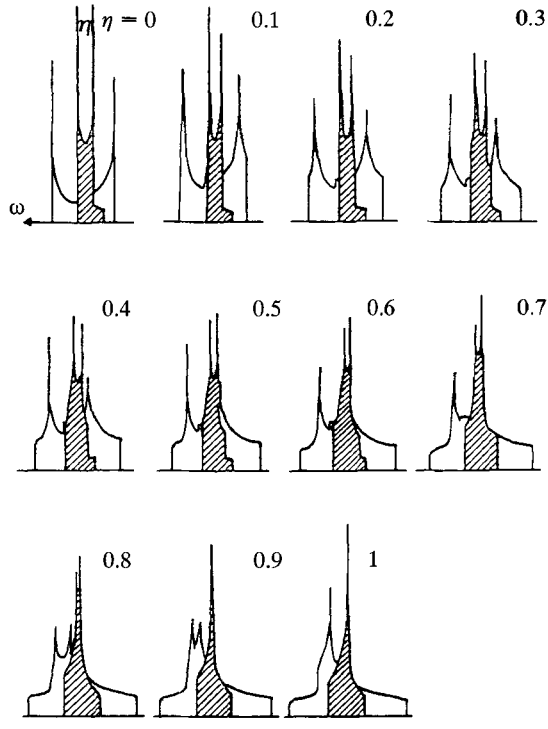


**Fig. 3.** The quadrupolar perturbed powder patterns of the $(1/2, -1.2)$ transition for various $\eta$ static (plain) and MAS (shaded). (From [16] with permission of Kluwer Academic publishers.)

(Fig. 4). This produces a frequency dependence for the $(m, m-1)$ transition:

$$\delta_{m,m-1} = \delta_{iso} + \delta_q^{(2)}, \tag{12}$$

where $\delta_q^{(2)}$ is the second-order quadrupolar contribution which for the central transition for $I = 5/2$ produces [15, 16, 27]:

$$\delta_q^{(2)} = \frac{9C_q^2}{800\nu_0^2}\left[-\frac{3}{5}\left(1+\frac{\eta^2}{3}\right)+\frac{1}{10}\left(-3+30\cos^2\vartheta-35\cos^4\vartheta\right)\right.$$

$$+\frac{\eta}{3}\left(1-8\cos^2\vartheta+7\cos^4\vartheta\right)\cos 2\varphi$$

$$\left.+\frac{\eta^2}{18}\left(\left(-3+10\cos^2\vartheta-7\cos^4\vartheta\right)\cos^2 2\varphi-\frac{4}{5}\right)\right] \tag{13}$$

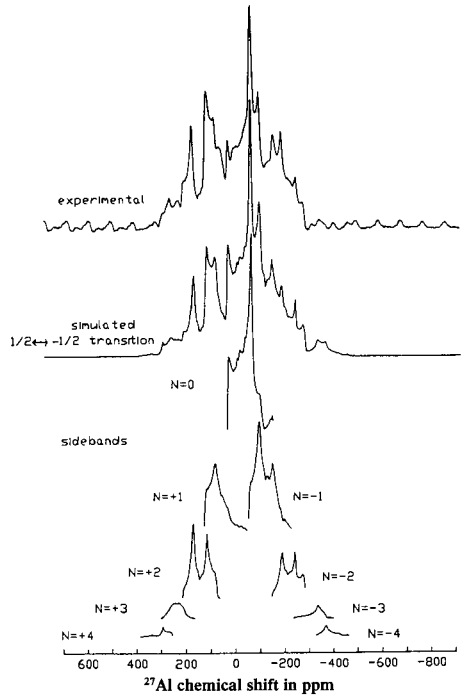


**Fig. 4.** The $^{27}$Al MAS NMR spectrum of $Al_2Ge_2O_7$ at 74.5 MHz and $\nu_r = 7$ kHz. (From [26] Massiot *et al.* Magn. Reson. Chem. **28**, S82 (1990) with permission of John Wiley and Sons Ltd.)

and this produces a second-order quadrupolar contribution to the isotropic shift of

$$\delta^{(2)}_{q,iso} = -\frac{3C_q^2}{16000\nu_0^2}(23 - 36m(m-1))(1 + \frac{\eta^2}{3}). \quad (14)$$

Although there is still a characteristic lineshape, the overall width under MAS is reduced by a factor of between 3 and 4 for the central transition, depending on $\eta$ (Fig. 3 [20]). The second-order width and shift of the peak depend on $C_q^2$ and $B_0^{-2}$ so that for large $C_q$ and low $B_0$ equating the peak position to $\delta_{iso}$ can be significantly in error. There is also a weak dependence on $\eta$ and stronger dependence on $m$ (Fig. 5). The $(\pm 3/2, \pm 1/2)$ transition is ~ 70% narrower and has only 12.5% of the isotropic second-order quadrupolar shift of the $(1/2, -1.2)$ transition (Table 1), so provided that sufficient intensity is present in the low order sidebands of this transition it can provide significant advantages in resolution and determination of $\delta_{iso}$ [27]. The aluminosilicate mineral leucite has three crystallographically distinct Al(4) sites but only two can be observed in the centreband of the $(1/2, -1/2)$ transition but the sidebands of the $(\pm 3/2, \pm 1/2)$

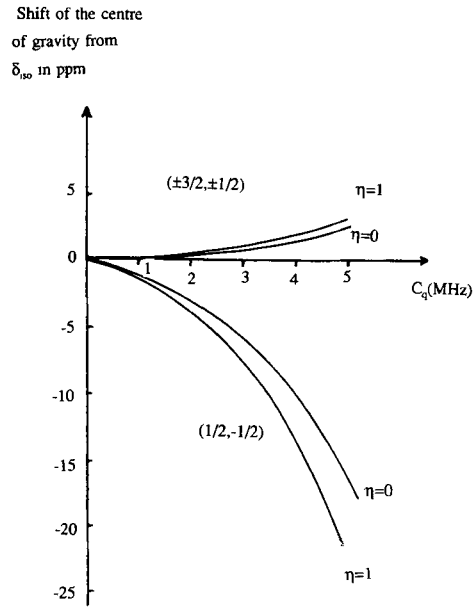


**Fig. 5.** The second-order quadrupolar shift of the centre of gravity away from $\delta_{iso}$ for the $(1/2, -1/2)$ and $(\pm 3/2, \pm 1/2)$ transitions for an $I = 5/2$ nucleus as a function of $C_q$ at 8.45 T.

transition clearly resolve all three sites (Fig. 6) [28]. Recording these satellite transitions has been used in the cases of albite [27], vesuvianite [29], thomsonite and scolecite [30].

For the more complex angular variation of the second-order term there are other choices of angle that minimize the broadening from it. The term variable angle spinning (VAS) is used to describe the studies of samples spin-

**Table 1.** Quadrupolar related spin properties of an $I = 5/2$ nucleus.

| Transition | All | $(1/2, -1/2)$ | $(\pm 3/2, \pm 1/2)$ | $(\pm 5/2, \pm 3/2)$ |
|---|---|---|---|---|
| $\lvert\langle m\rvert I_+\rvert m-1\rangle\rvert^2$ | n.a. | 9 | 8 | 5 |
| Peak pulse intensity | 1 | 0.086 | 0.081 | **0.064** |
| Short rf-pulse intensity | 1 | 0.257 | 0.228 | 0.143 |
| 90° pulse length | 1 | 0.333 | 0.354 | 0.442 |
| Isotropic second-order quadrupolar shift* | n.a. | 1 | −0.125 | −3.5 |
| Second-order quadrupole linewidth* | n.a. | 1 | 0.292 | 1.83 |
| Intensity of low order sidebands* | n.a. | 1 | 0.12 | 0.006 |

* Relative to the $(1/2, -1/2)$ transition, for details see [27].

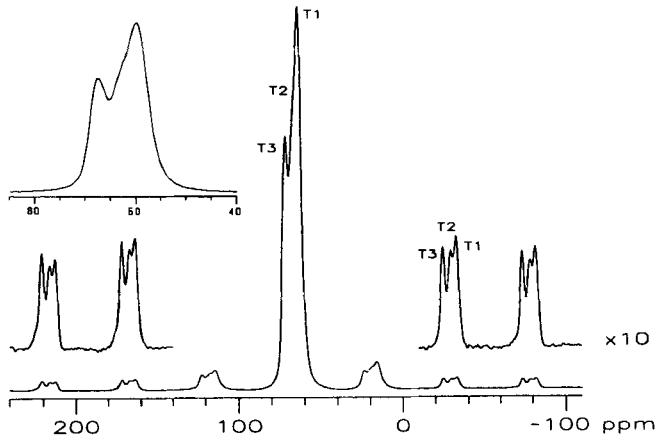


**Fig. 6.** $^{27}$Al MAS NMR spectrum of leucite 999 showing the enhanced resolution in the sidebands of the (±3/2, ±1/2) transition. (From [24] with permission of Springer Verlag.)

ning at angles other than 54.7° [25, 31–34]. In the range 60°–70° the minimum width is obtained (depending on $\eta$) and at 43.5° the lineshape becomes independent of $\eta$ [33]. Calculations of the intensity distribution of the spinning sideband intensity have also been performed [25, 34]. VAS is useful when the sources of linebroadening other than the quadrupolar interaction are negligible but unfortunately for $^{27}$Al this is not often the case.

It would clearly be desirable to remove both first-order and second-order terms simultaneously and recently schemes have been devised to achieve such averaging [35, 36]. As no single rotation axis can remove both the terms proportional to $P_2(\cos\vartheta) = 1/2(3\cos^2\vartheta - 1)$ and $P_4(\cos\vartheta) = 1/8(35\cos^4\vartheta - 30\cos^2\vartheta + 3)$ the axis direction must be made time-dependent. Two distinct schemes have been developed. One scheme, termed dynamic angle spinning (DAS) flips the rotation axis between two different angles $\vartheta_1$ and $\vartheta_2$ to the applied field so as to satisfy $P_2(\cos\vartheta_1) = -kP_2(\cos\vartheta_2)$ and $P_4(\cos\vartheta_1) = -kP_4(\cos\vartheta_2)$. There are a continuum of solutions depending on the relative time spent at each angle. In the case of equal times, $\vartheta_1 = 37.38°$ and $\vartheta_2 = 79.19°$. The data is collected either as a one-dimensional data set of the echo amplitude as a function of the evolution time; or as a two-dimensional NMR data set with the f2-dimension containing the complete spectrum (the data after the echo) while the f1-dimension (the evolution time) contains only isotropic information [37]. The alternative method (DOR) is to make the direction of the spinner axis continuously variable by having a spinner within a spinner, both of which rotate. The effect of such rotation on the Hamiltonian can be derived from Eq.(11) by having three successive rotations; from the PAS to the first rotor, then to the second rotor and finally to the laboratory. The two angles which have to be set to remove both first and second order effects are the angle between the two rotor axes and the

outer rotor and $B_0$. They are set so as to solve $P_2(\cos\vartheta_1) = 0$ (i.e. $\vartheta_1 = 54.7°$) and $P_4(\cos\vartheta_2) = 0$ (i.e. $\vartheta_2 = 30.56°$ or $70.17°$) [38].

The other main difference between quadrupolar nuclei and spin-1/2 nuclei is that their pulse response depends on $C_q$ which has been discussed in a number of theoretical papers [23, 39–44]. The intensity is spread amongst the five transitions, each of which has an inherent quantum intensity fixed by the matrix element $|\langle m|I_+|m-1\rangle|^2$ (Table 1 [39]). There are two limiting cases either $\nu_q \gg \nu_1 (= \gamma B_1/2\pi)$ and the central transition is well separated from the outer ones and the pulse response is $A\sin A\omega_1 t_p$ (where $A = [I(I+1) - m(m-1)]^{1/2}$ and $t_p$ is the pulse duration). The magnetization corresponding to the different transitions behaves effectively as an independent spin-1/2 nucleus but with its gyromagnetic ratio enhanced, and intensity diminished by a factor $A$ and is termed a fictitious spin-1/2 system [13]. This has been accurately demonstrated using a single crystal of $\alpha$-$Al_2O_3$ by putting each of the transitions on resonance in turn [45]. In the other limit where $\nu_q \ll \nu_1$ the energy levels becomes almost equally spaced and hence the transitions are degenerate and the nucleus behaves as a spin-1/2 nucleus with the same gyromagnetic ratio and response $A^2\sin\omega_1 t_p$. Between these two extremes the pulse response becomes complex and non-sinusoidal [23, 39, 43] (Fig. 7). A comparison of $Al(NO_3)_3$ in aqueous solution ($C_q \sim 0$) and $Y_3Al_5O_{12}$ which has Al(4) ($C_q = 6$ MHz) and Al(6) ($C_q = 0.6$ MHz) provides examples of all three cases for which the effective 90° pulses and intensities are clearly seen to be different.

These effects have some important consequences for conducting experiments so as to obtain quantitatively reliable data. If $C_q$ is known then any pulse-length can be used with suitable correction. To allow direct comparison that does not demand accurate knowledge of $C_q$ the small pulse angle limit should be used (Fig. 7). Then the approximation $\sin x \sim x$ is valid and in both $\nu_q$ limits the observed intensity tends to $A^2\omega_1 t_p$. For less than 5% error in quantitative comparison [30]:

$$(I+\frac{1}{2})\omega_1 t_p < \frac{\pi}{6}. \tag{15}$$

The $C_q$-dependence of the pulse response can be useful for discriminating sites with differing $C_q$ that overlap in one-dimensional NMR spectra, and to a limited extent can be used to determine $C_q$. This is the basis of the 2D nutation method [46, 47].

The efg is produced by a non-uniform distribution of charge outside the nucleus such as surrounding ions and bonding electrons. The $r^{-3}$ dependence of this effect means that charges closest to the nucleus are most significant. The charges outside the inner spherical charge shells of the atom produce a field gradient $q'$ but when this impinges upon the electrons their spherical

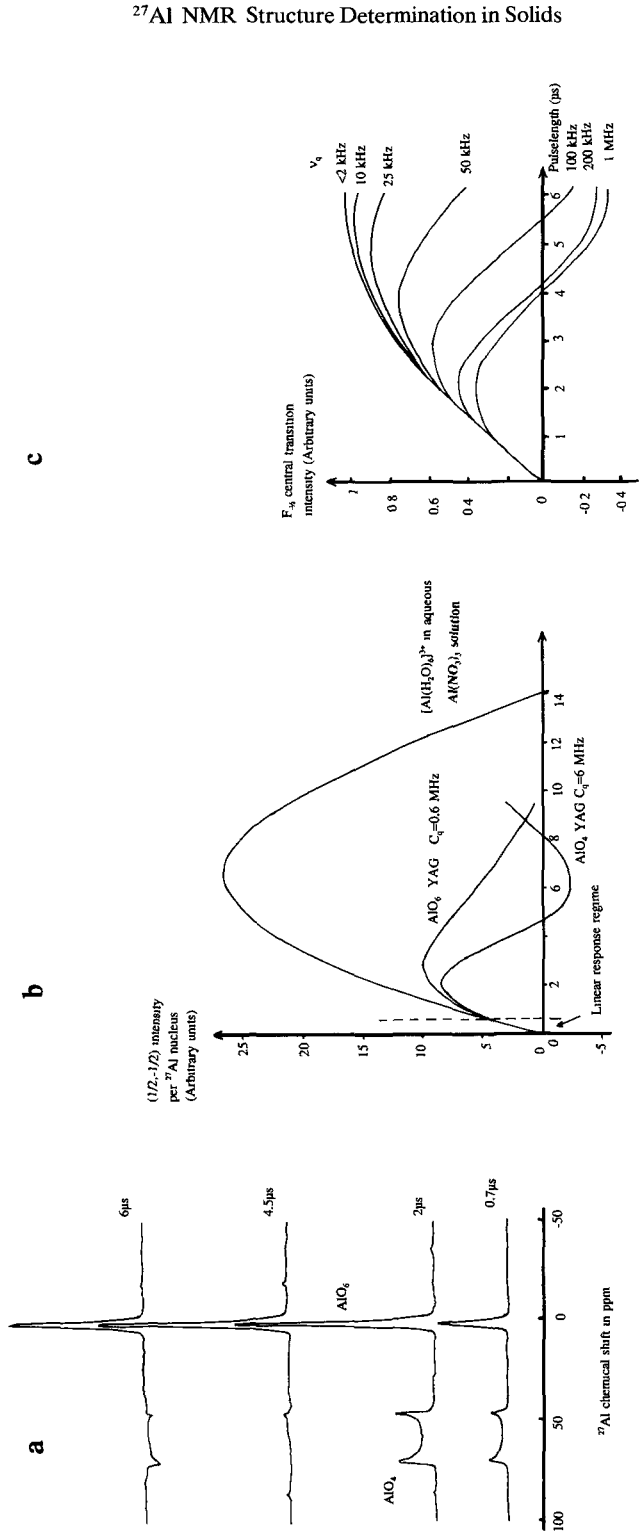


**Fig. 7.** **a** 9.4 T $^{27}$Al MAS NMR spectra of $Y_3Al_5O_{12}$ as a function of pulselength and **b** full experimental response curves compared to an aqueous solution of aluminium nitrate with $B_1 = 5$ mT. **c** Theoretical response for an $I = 5/2$ nucleus to a $B_1 = 3.8$ mT for various $\nu_q$. (Part **c** with permission of Elsevier Science Publishers from [41].)

distribution will distort to minimize their own energy, thereby enhancing the efg at the nucleus. This can be significant due to their proximity to the nucleus and is described by the Sternheimer antishielding factor $\gamma_\infty$ [48, 49]:

$$\underline{q} = (1 - \gamma_\infty)\underline{q'}. \tag{16}$$

This factor is always present in the measured values of $q$, and can be regarded as approximately constant for a particular element (for $^{27}Al$ as $Al^{3+}$ $\gamma_\infty = -3.61$ [50]) so does not complicate comparison between samples. However for heavier elements it can become very much larger and makes comparisons of the site distortions for different elements far from straightforward.

The quadrupolar nature of $^{27}Al$ can also effect the spectra of spin-1/2 nuclei with which it interacts since if the quadrupolar interaction becomes sufficiently large compared to the Zeeman interaction $m$ is no longer a good quantum number for the aluminium spin states and MAS can only partially remove dipolar and J-coupling interactions [51]. Usually $\nu_q \ll \nu_0$ so that these residual effects are seldom observed but reports exist of the distortion of the $^{31}P$-$^{27}Al$ J-coupled sextet in the complex $(CH_3)_3P$-$AlCl_3$ in dehydrated Na-HY zeolite [52] and in a very pure sample of kyanite where paramagnetic broadening was not the limiting factor two distinct $^{29}Si$ could be resolved at high field [53].

## 3. Experimental Methods

One pulse acquisition experiments in conjunction with MAS are the most common for $^{27}Al$ NMR studies of solids, and careful thought has to be given to the extraction of the data from such experiments. To fully interpret any spectrum it is a prerequisite that $C_q$, $\eta$ and $\delta_{iso}$ are known. Methods available to extract these parameters include:

(1) Observation and simulation of second-order quadrupolar lineshapes of the $(1/2, -1/2)$ transition for either static or MAS cases.

(2) Observation and simulation of the first-order spectra from the non-central transitions for static or MAS cases to determine $C_q$ and $\eta$ and the centre of gravity of the $(\pm 3/2, \pm 1/2)$ transition to estimate $\delta_{iso}$.

(3) The field dependence of the $(1/2, -1/2)$ transition with $B_0$.

(4) The 2D pulse response nutation experiment.

(5) Application of VAS, DAS or DOR techniques.

If a second-order quadrupolar powder pattern can be clearly observed for the central transition all parameters can be unambiguously extracted. Static

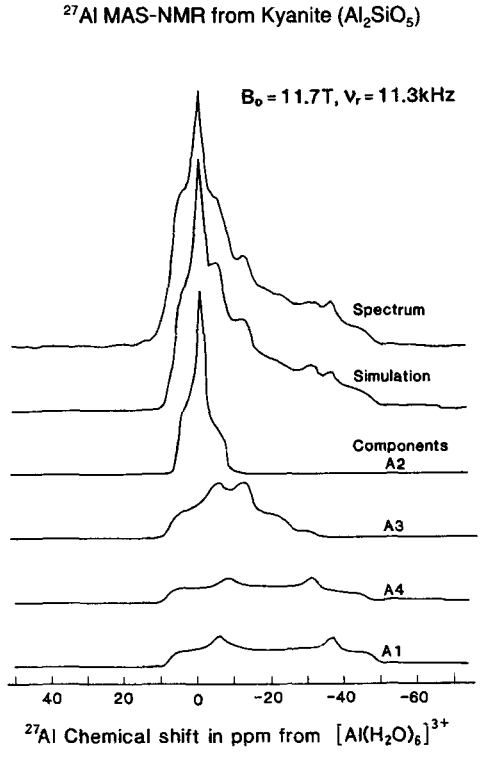


**Fig. 8.** $^{27}$Al MAS NMR spectrum of kyanite at 11.7 T and $\nu_r = 11.3$ kHz together with a spectral simulation.

spectra tend to be smoothed and suffer from increased overlap in the cases when multiple sites are present hampering extraction of the parameters. MAS improves both of these points and the spectrum of kyanite (a polymorph of $Al_2SiO_5$, Fig. 8) clearly shows four sites (Table 2). The ability to produce such a spectrum has only recently become possible because of the

**Table 2.** Simulation parameters, integrated spectral intensity, magnetization in the centreband and corrected intensity for the $^{27}$Al MAS NMR spectrum of kyanite.

| Site | $C_q$ (MHz) | $\eta_q$ | $\delta_{iso}$ (ppm) | Integrated intensity of the centreband | Fraction of (1/2, −1/2) transition in the centreband | Corrected spectral intensity |
|---|---|---|---|---|---|---|
| A2, $AlO_6$ | 3.7 | 0.89 | 5 | 0.29 | 1.00 | 0.26 |
| A3, $AlO_6$ | 6.53 | 0.59 | 7.5 | 0.29 | 0.95 | 0.27 |
| A4, $AlO_6$ | 9.37 | 0.38 | 13 | 0.20 | 0.81 | 0.22 |
| A1, $AlO_6$ | 10.03 | 0.27 | 15 | 0.22 | 0.78 | 0.25 |

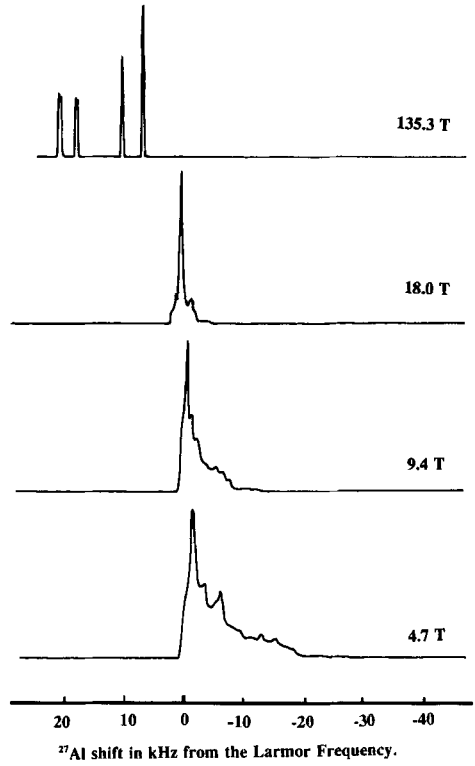


**Fig. 9.** Simulations of the $^{27}$Al fast MAS NMR spectra of kyanite as a function of applied magnetic field.

combination of fast MAS and high $B_0$ [54–59]. The resolution improves as $B_0^2$ and Fig. 9 shows the effect on simulated spectra of kyanite. Between 4.7 and 9.4 T the bandshape is almost identical except scaled by a factor of two. As the most shielded sites A1 and A4 have the larger $C_q$ at these fields their centres of gravity are at more deshielded values. However as $B_0$ increases the centre of gravity approaches $\delta_{iso}$ and at 135.3 T four clearly resolved lines exist, but note at the intermediate field of 18 T there is considerable overlap which is a result of the relative $\delta_{iso}$ and $\delta_{q,iso}{}^{(2)}$ at this field.

The residual second order width under MAS for the central transition is [16, 58]:

$$\Delta\nu_{MAS}{}^{(2)} = \frac{C_q^2}{2850\nu_0}(6+\eta)^2 . \tag{17}$$

This is often significant compared to $\nu_r$ and for the centreband to be unencumbered by spinning sidebands and to effectively produce some narrowing

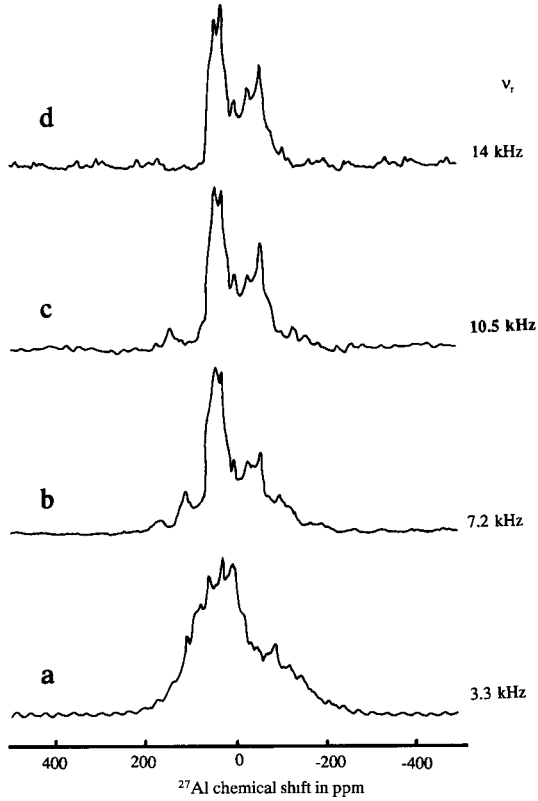


**Fig. 10.** $^{27}$Al MAS NMR spectra of sillimanite at 9.4 T as a function of $\nu_r$.

requires $\nu_r \gg \Delta\nu_{MAS}$[2]. Failure to satisfy this can lead to an unnarrowed and consequently broad line that could be lost from the spectrum. Andalusite (another polymorph of $Al_2SiO_5$) has attracted much attention because it has a well defined Al(5) site. It also has an Al(6) site with $C_q = 15.6$ MHz (Table 4). Early MAS work using moderate spinning speeds (< 4 kHz) could only reveal the Al(5) site with the only evidence for the other aluminium species being a broad underlying resonance [60, 61]. Subsequent studies at higher fields (> 11.7 T) and faster MAS (> 15 kHz) showed both lines [59, 62, 63]. The effect of $B_0$ and $\nu_r$ can be appreciated by considering 4 kHz at a field of 7.05 T where the largest $C_q$ that gives a centreband free from sidebands is 4.9 MHz while for 15 kHz at 11.7 T this has increased to 12.3 MHz (assuming $\eta = 0$). This is illustrated by the evolution with spinning speed of the spectrum of sillimanite, the third polymorph of $Al_2SiO_5$, at 9.4 T. There are Al(4) and Al(6) sites which under sufficiently rapid MAS produce second-order widths for the centreband of 6.7 and 11.4 kHz respectively. At 3.3 kHz (Fig. 10a) very limited narrowing occurs and a complex overlapping bandshape is obtained. 7.15 kHz exceeds the residual

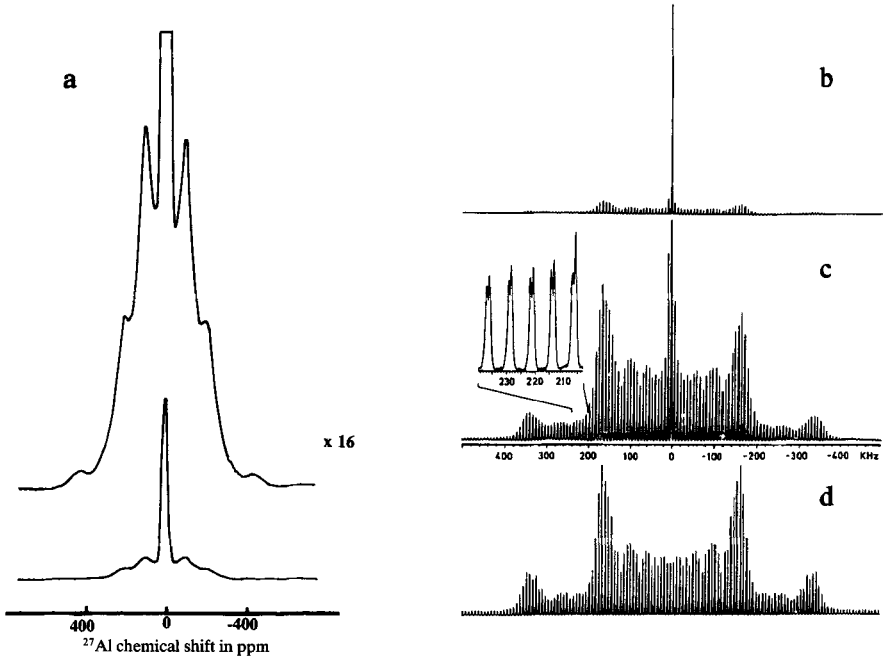


**Fig. 11.** **a** The static 9.4 T NMR spectrum of $LaAlO_3$ ($C_q = 0.12$ MHz) showing all the transitions and **b**, **c** MAS spectra of $\alpha$-$Al_2O_3$ showing the narrowed outer transitions with an intensity envelope similar to the static pattern and **d** a simulation. (**b**–**d** from [66] with permission of Academic Press.)

width for the Al(4) site and the comparatively narrow resonance from this site is now dominant, but little narrowing of the Al(6) site occurs (Fig. 10b). However by 14 kHz (Fig. 10d) both sites have narrowed and can clearly be distinguished. It is important to recognize that these effects are particularly important in disordered materials where a range of $C_q$ and $\eta$ are present so that at different fields and spin rates significantly different spectra can be obtained as differing fractions of the sites narrow.

For smaller $C_q$ (< 2.5 MHz) the second-order structure is often too small to be resolved even under MAS. However the first-order width is now not prohibitively large so that pulse methods can be used and lineshapes obtained (Fig. 11a). Fast MAS accurately at the magic angle can cause dramatic narrowing of the outer transitions into a set of sharply defined spinning sidebands whose intensity envelope closely follows the static lineshape. This improves the resolution and means that from the $(\pm 3/2, \pm 1/2)$ transition $\delta_{iso}$ can also be more accurately determined. To narrow such broad resonances requires accurate setting and high stability of the magic angle. Suppose that the angle is slightly misset by $\xi$, so spinning is at $(\beta + \xi)$, this produces a residual width of

$$\Delta\nu_{mis} = 3\cos\beta\sin\beta\Delta\nu_{stat}\,\xi\,. \tag{18}$$

As the static width ($\Delta\nu_{stat}$) becomes large the accuracy of the setting of the magic angle becomes increasingly crucial so that standard compounds such as KBr [64] are not sensitive enough and the angle should be calibrated on each compound. Other experimental considerations include the effects of the delay in recording the start of the free induction decay (FID) after the pulse and the rf-excitation profile of the pulse both of which can be modeled as sinc functions [26, 59, 65]. The digitization of the signal can also be a problem in that narrow spectral features (the sidebands) are spread over a broad frequency range. In the time domain this means very short lived rotational echoes have to be rapidly digitized to accurately determine the intensity envelope of the spinning sidebands but the acquisition time must be long enough to capture the whole of the slowly decaying component and prevent truncation. These two criteria often exceed the capabilities of most digitizers available, even for spectrometers designed for solids. However the first-order singularities in the sideband pattern from $\alpha$-$Al_2O_3$ where $C_q = 2.38$ MHz can be clearly observed (Figs. 11b − 11d) [66, 67] and has been applied to other compounds [67, 68].

It is apparent that second-order lineshapes from the central transition are often obscured leaving slightly asymmetric Gaussian lineshapes. Some work has estimated a correction to the peak position to find $\delta_{iso}$ using this linewidth [69] but as this width usually contains contributions other than quadrupolar, tending to make $\delta_{iso}$ too paramagnetic [30]. The change of peak position (or more correctly the centre of gravity) with $B_0$ is a good way to estimate $\delta_{iso}$. The shift of the centre of gravity is:

$$\delta_{cg} = \delta_{iso} - \frac{3\pi^2 C_q^2 (1 + \frac{\eta^2}{3})}{125\gamma^2 B_0^2}\,. \tag{19}$$

A typical set of data shows the peak position (in ppm) plotted against $B_0^{-2}$ for the clay mineral kaolinite (Fig. 12) producing a very good straight line. The gradient is proportional to $C_q(1 + \eta^2/3)^{1/2}$; this combination is sometimes termed the second-order quadrupole effect parameter [58, 70]. Either this product can be quoted or some approximation for $\eta$ made. As long as any assumption is clearly stated the data is useful; $\eta = 0.67$ gives the smallest maximum error in $C_q$ of 15%. The intercept at $B_0^{-2} = 0$ (a poor man's way of getting very high field data) gives $\delta_{iso}$. The linewidth variation of MAS spectra with field can also provide information as there are usually two main contributions: the residual second-order quadrupolar width and dispersion of the isotropic chemical shift ($\Delta\nu_{dis}$) so that the half width can be written as:

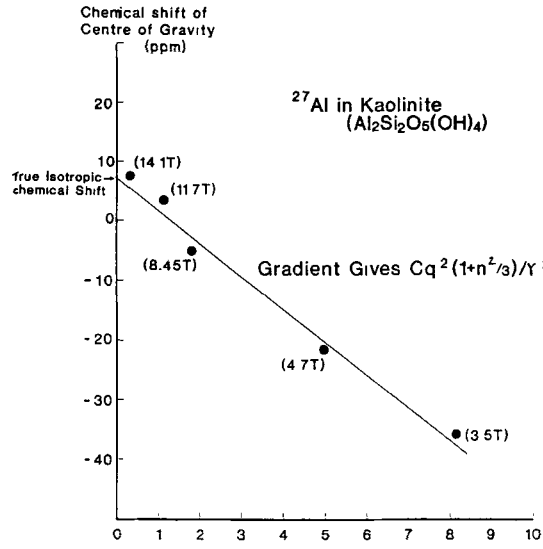


**Fig. 12.** Peak position of the $^{27}$Al NMR from kaolinite plotted as a function of $B_0^{-2}$.

$$\Delta\nu_{1/2} = \Delta\nu_q^{(2)} + \Delta\nu_{dis} \,. \tag{20}$$

$\Delta\nu_q^{(2)}$ decreases inversely and $\Delta\nu_{dis}$ (in Hz) increases directly with $B_0$. For glasses and zeolites $^{27}$Al MAS spectra at high field have linewidths dominated by chemical shift dispersion [71, 72]. This information is useful in characterizing "disorder" in solids.

If $C_q$ is such that $\nu_q \sim \nu_1$ an alternative approach to estimate $C_q$ is to follow the pulse response. This has been developed into the simple but effective two dimensional quadrupolar nutation sequence with the second time dimension simply being the pulselength. This experiment separates the spectral information so that the normal, high field spectrum lies in f2 and along f1 there is quadrupole excitation information. While the pulse is on $B_1 \sim 0.001 B_0$ the experiment is effectively a low field experiment with the spin states determined by the quadrupolar interaction, while retaining high field sensitivity. In the limits $\nu_q \ll \nu_1$ and $\nu_q \gg \nu_1$ the f1 response lies at $\nu_1$ and $3\nu_1$. However in the intermediate regime where $\nu_q \sim \nu_1$ the response is complex but allows deduction of $C_q$ and $\eta$ by comparison with theoretical simulations (Fig. 13). Nutation experiments are usually performed on static samples but can be combined with MAS provided that $t_p < t_r/4$ [47].

The question of quantification of aluminium spectra has caused much discussion, with for example dealuminated zeolites sometimes showing significant loss of signal intensity, corresponding to distorted sites producing so called "NMR invisible" aluminium. Comparison can be made to a standard compound (e.g. $\alpha$-$Al_2O_3$ [73, 74], 1 M $AlCl_3$ aqueous solution [75]) to see

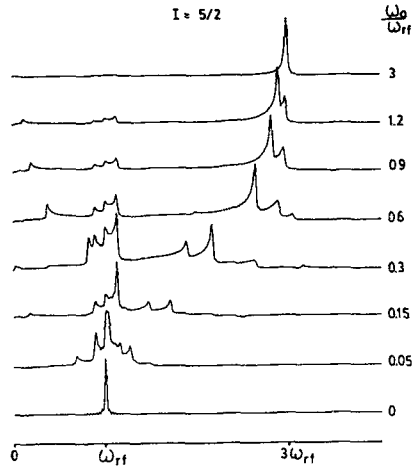


**Fig. 13.** Theoretical nutation spectra for $I = 5/2$ as a function $(\omega_q/\omega_{rf})$. (Note that the vertical scales are not equivalent, taken from [46] with permission of Academic Press.)

how much signal is being lost. Differing $T_2^*$ leads to differential signal loss during the initial system recovery time which can be compensated for by extrapolation to $t = 0$ but very broad spectral components can be completely lost. Most work has shown that with higher magnetic fields and better spectrometer technology, allowing more rapid recovery, these problems are much diminished, but it is crucial for any work in this area to quote the pre-acquisition delay to allow the quality of the data to be assessed. In quantification of work at slower spinning speeds when both Al(4) and Al(6) were present overlap of sidebands often hampered accurate deconvolution. The TOSS pulse sequence was used to produce sideband free spectra and reveal partially obscured peaks [76]. Much of the earlier spectra could be usefully repeated with the more rapid rotation rates now available.

Spectra accumulated in the linear regime (Fig. 7) with fast MAS and rapid system recovery while being quantitative still present the difficulty of estimating the fraction of magnetization present in the centreband. Why not simply integrate over sidebands as well as the centreband as for spin-1/2 nuclei? The difficulty is that there is no necessity for these to have the same lineshape (Fig. 4) and the sidebands can be as broad as the centreband but with only (5−10)% of the intensity, with the added difficulty of the superposition of the sidebands from the non-central transitions. This can make their integration very much less accurate than that for the centreband, which could be corrected by knowing the amount of magnetization present. For the $(1/2, -1/2)$ transition this amount depends on the parameter $(\nu_q^2/\nu_0\nu_r)$ and for the outer transitions $(|1 - 2m|\nu_q/\nu_r)$ and weakly on $\eta$ (Figs. 14a and 14b) [77]. Kyanite (Fig. 8) has four equally populated Al(6) sites but direct integration of the centrebands gives intensities in the range (20−30)%

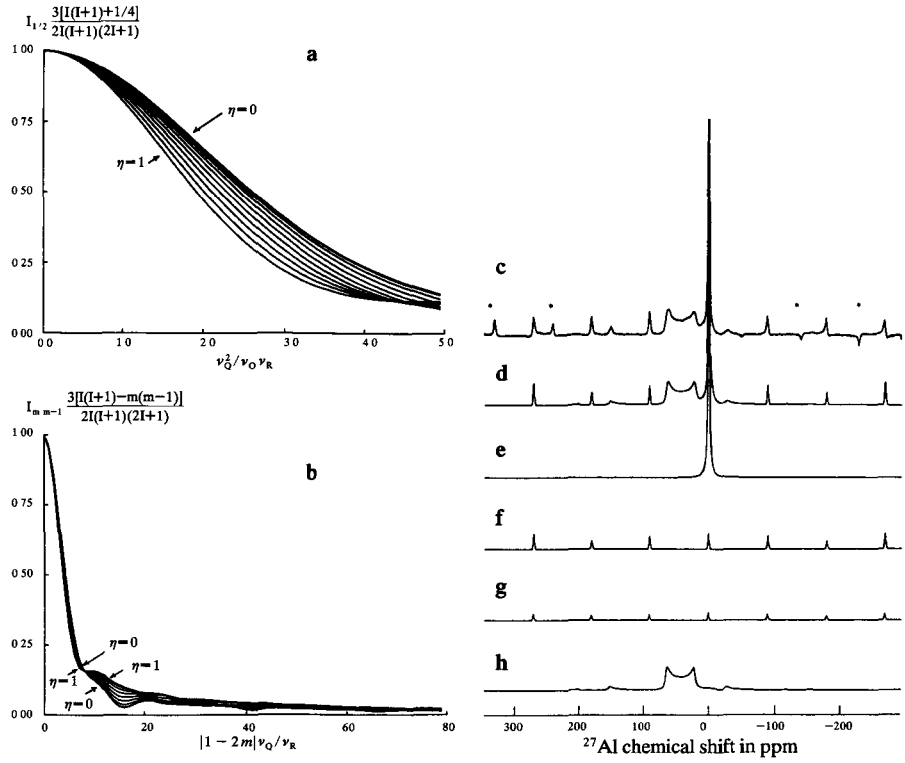


**Fig. 14.** Theoretical plots of the fraction of the magnetization in the centreband as a function of $\nu_q$ and $\nu_r$ for **a** the central transition and **b** the outer transitions. **c** The $^{27}$Al MAS NMR spectrum at 7.05 T and 7 kHz for $Y_3Al_5O_{12}$ together with a simulation of **d** the complete spectrum as well as the components for Al(6) **e** $(1/2, -1/2)$ transition, **f** $(\pm 3/2, \pm 1/2)$ transitions and **g** $(\pm 5/2, \pm 3/2)$ transitions and **h** Al(4) $(1/2, -1/2)$ transition. (From [77] with permission of Academic Press.)

(Table 2) [59]. It can be seen (Table 2) that the sites with larger $C_q$ have the lower apparent intensity but correcting using Fig. 14a shows that all sites more closely approach 25% (Table 2).

In the case of kyanite, only the central transition contributes significantly to the centreband (cb). $Y_3Al_5O_{12}$ provides a more interesting case where the two sites Al(4) and Al(6) have very different quadrupolar parameters (Table 4). Integration of the centreband gives 1 : 1 whereas from the structure it should be 3 : 2. For the Al(6) site, since the quadrupolar interaction is small the intensity ($In$) contribution from the non-central transitions can no longer be neglected:

$$In_{cb} = \sum_{m=-I}^{I-1} In_{cb}^{m} . \tag{21}$$

**Table 3.** Intensity correction factors from different transitions for the $^{27}$Al centrebands of $Y_3Al_5O_{12}$.

| Site | $AlO_4$ | $AlO_6$ |
|---|---|---|
| $\nu_q$ (kHz) | 900 | 90 |
| $\delta_{iso}$ (ppm) | 76.0 | 0.8 |
| Integrated intensity of centreband (relative) | 1 | 1 |
| Transition (1/2,−1/2) | | |
| $\nu_q^2/\nu_0\nu_r$ | 1.48 | 0.15 |
| Inherent intensity | 1 | 1 |
| Fraction contributed to centreband | 0.78 | 1 |
| Transition (3/2,1/2) + (−3/2,−1/2) | | |
| $\lvert 1-2m\rvert\nu_q/\nu_r$ | 257 | 25.7 |
| Inherent intensity | 1.78 | 1.78 |
| Fraction contributed to centreband | 0 | 0.045 |
| Intensity contributed to centreband | 0 | 0.08 |
| Transition (5/2,3/2) + (−5/2,−3/2) | | |
| $\lvert 1-2m\rvert\nu_q/\nu_r$ | 514 | 51.4 |
| Inherent intensity | 1.11 | 1.11 |
| Fraction contributed to centreband | 0 | 0.3035 |
| Intensity contributed to centreband | 0 | 0.039 |
| Total contributed intensity | 0.78 | 1.12 |
| Corrected centreband intensity (relative) | 1.28 | 0.89 |

An experiment carried out at 78.21 MHz and $\nu_r = 7$ kHz (Fig. 14c) [77] results in only 78% of the central transition intensity in the centreband of the Al(4) site and no contribution from the outer transitions (Table 3). For the Al(6) site all the $(1/2, -1/2)$ magnetization is in the centreband and there is also a significant contribution from the outer transitions. After suitable weighting by the inherent quantum intensity (Table 1) the non-central transitions contribute an additional 12% to the centreband (Table 3). The corrected intensities produce Al(4) : Al(6) of 1.28 : 0.89, very close to the crystal structure.

Of course to get quantitative information, it is implicit that sufficient recycle delay is used to prevent saturation of the magnetization. In general $^{27}$Al relaxation is fast with $T_1$ often less than 1 s, being ~ 1 ms [78] for some zeolites, but it can be as long as 20 s in some ceramics. For quadrupolar nuclei the relaxation is often multicomponent which comes from there being more than two energy levels [65, 79]. MAS can complicate determination of $T_1$ as the pulse usually excites all nuclei in the central transition but only a small fraction of the non-central transition. In the case of a 90°−$\tau$−90° sequence nuclei excited by the first pulse will not necessarily be the same subset excited by the second because the orientation of the rotor will have changed. Measurement of $^{27}$Al relaxation in albite showed that a saturating comb always gave a longer $T_1$ value than the 90°−$\tau$−90° sequence [80]. Dif-

ferences were also noted between static ($T_1$ = 8.8 s) and MAS ($T_1$ = 19.4 s) experiments [80].

The high natural sensitivity of $^{27}Al$ means that cross-polarization (CP) has been seldom employed but $^{1}H$-$^{27}Al$ [81–84] and $^{19}F$-$^{27}Al$ [85] have been reported. A weaker signal than for the one pulse experiment is usually obtained due to the distribution of nuclei and the spin dynamics. The selectivity of the experiment preferentially polarizes those nuclei close to the polarizing nucleus at short contact times and means that minor resonances in the direct spectrum may be enhanced. For a quadrupolar nucleus the Hartmann-Hahn condition has to be modified in the case that $C_q$ is large to take into the account the effective gyromagnetic ratio so that for the central transition:

$$3\gamma_{Al} B_1^{Al} = \gamma_x B_1^x . \tag{22}$$

For $^{1}H$-$^{27}Al$ CP aluminium hydroxide and kaolinite have been used as set-up compounds. It should be noted that $T_{1\varrho}$ obtained from MAS experiments may be spurious as when $\nu_r \sim \nu_{eff}$ (due to the spin-lock pulse) sizeable excursions out of the transverse plane may occur so that nuclei are unable to follow the spin-lock field [82]. Applications of CP are discussed below.

## 4. The Al-O-H System

Aluminas are widely used as a catalysts and catalyst supports. $\alpha$-$Al_2O_3$ is formed by calcination of the hydroxides (bayerite, gibbsite) and oxyhydroxide (boehmite) causing dehydroxylation and proceeds via various intermediate aluminas [3, 6, 86, 87]. Calcination produces changes in the structure mirrored in the fraction of Al(6) sites, with MAS NMR spectra giving 0.94 for AlO(OH), 0.75 for $\gamma$-$Al_2O_3$ and 1 for $\alpha$-$Al_2O_3$ (Fig. 1c) [3, 86]. The transitional aluminas have close-packed oxygens in a spinel-like structure with aluminium and vacancies distributed over the interstitial octahedral and tetrahedral sites. A fractional Al(6) content for $\gamma$-$Al_2O_3$ of 0.75 confirms Lippen's model for the structure with all the vacancies ordered onto the tetrahedral sites [6]. Calcination of hydragillite produces a very poorly crystalline intermediate state with three peaks at 3, 35 and 64 ppm which were assigned to Al(6), Al(5) and Al(4). Further heating causes conversion into $\eta$-$Al_2O_3$ and eventually $\alpha$-$Al_2O_3$ [88]. Revisiting these materials using rapid MAS (> 10 kHz) to remove all the sidebands from the isotropic region has produced clearer spectra. Dehydroxylation of gibbsite was followed in detail with Al(6) and Al(4) sites apparent. However the spectra often are not simple superpositions of spectra of the constituent phases as broad unnarrowed components are present. $\varrho$-alumina, known from XRD to be highly disordered, showed a third peak at 27 ppm, probably due to Al(5). Calcines

derived from gibbsite at (900–1000)°C, with significant χ-alumina content showed some interesting structure in the Al(4) region with a peak/shoulder at 45 ppm although its source was not identified [89].

High surface area aluminas tend to show a decrease in the observable aluminium intensity with increasing surface area [90]. CP experiments preferentially enhance surface species and both Al(4) and Al(6) are observed, but the latter more strongly so. γ-$Al_2O_3$ produced a stronger CP signal than α-$Al_2O_3$ which was interpreted as being due to a higher number of Bronsted acid sites on γ-$Al_2O_3$. A surface area of at least (2–3) $m^2g^{-1}$ is necessary to allow observation of surface species [81]. Examination of various transitional aluminas which had molybdenum deposited on the surface indicated the formation of $Al_2(MoO_4)_3$ [91].

The aluminium species present in aqueous solution have a profound effect on the oxides/hydroxides which precipitate out. Normally $[Al(H_2O)_6]^{3+}$ is present but is replaced at higher pH by $[Al(OH)_4]^-$. More complex species can also be present such as the tridecameric cation $[Al_{13}O_4(OH)_{24}(H_2O)]^{2+}$ and narrow NMR signals from Al(4) species at 62.4 ppm and a much broader Al(6) peak at 8 ppm have been observed [92].

Sol-gel preparations of aluminas from both boehmite and aluminium sec-butoxide showed the formation of γ-$Al_2O_3$ [93] but with different Al(4)/Al(6) ratios suggesting differing orderings of the cations. Gelation of sols shows two Al(6) sites initially form at 8 ppm ($\Delta\nu_{1/2}$ ~ 90 Hz) and 0 ppm ($\Delta\nu_{1/2}$ ~ 2200 Hz). Addition of $HNO_3$ rapidly enhances the peak at 0 ppm at the others expense as the aluminium sol-polymers form a more extensive amorphous gel network [94]. Calcination of dehydrated gel powders formed from aluminium proponiate at 800°C showed that an unsonicated powder gave α-$Al_2O_3$ while a sonicated powder produced γ-$Al_2O_3$ [95]. A comparison of a series of transitional alumina gels prepared with differing crystallinity and morphology showed concomitant changes in the surface properties. An amorphous sample showed lower activity, which could be correlated to a smaller number of Al(4) sites [96]. Precursor solutions ($Al(OPr)_3$-$AlCl_3$-citric acid-$H_2O$) for alumina fibre formation contain predominantly Al(6), but at least three distinct sites were observable. Only the initial stages of reaction were followed and further work to examine changes of the fibre structure with heat treatment would be valuable [97].

Protection of aluminium with anodically deposited thin oxide films offers significant improvements in corrosion resistance. The largely amorphous layer has a hexagonal pore structure with the wall being almost pure alumina and the intermediate region contaminated by the electrolyte. MAS NMR spectra show three narrow resonances at 4, 30 and 63 ppm assigned to Al(6), Al(5) and Al(4) on the top a broader resonance (Fig. 15) [6]. As the rotation rate is increased and more nuclei satisfy the condition that $\nu_r \gg \Delta\nu_{MAS}^{(2)}$, the intensity in the broader component is reduced but the larger $\Delta\nu_{MAS}^{(2)}$ means that the apparent resolution of the sharp components

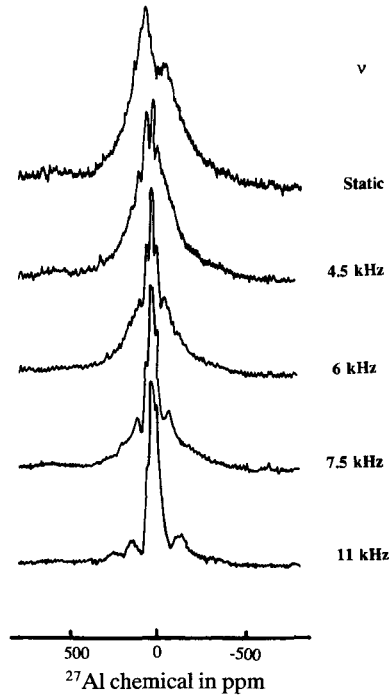


**Fig. 15.** $^{27}$Al MAS NMR spectra of an anodic alumina barrier film at 8.45 T at various spin rates.

is degraded. Films prepared with chromic acid as the electrolyte are thought to be more ordered and only showed a narrow Al(6) resonance. Others prepared from phosphoric, oxalic and sulphuric acids have a decreasing cell wall thickness that was correlated with an increase in the Al(6) content of the spectra [98].

## 5. Aluminates

Distinguishing between Al(4) and Al(6) species in simple aluminates was one of the earliest applications of $^{27}$Al MAS NMR [2, 5]. $\delta_{iso}$ for $^{29}$Si is known to be sensitive to the connectivity of the constituent tetrahedra (referred to as a $Q^n$ species, where n is the number of bridging bonds; see [99]). For $^{27}$Al careful correction of the peak position is necessary (*vide supra*). $\delta_{iso}$ clearly distinguishes Al(4) and Al(6) (Fig. 16) as well as Al(4) with either Al(4) or Al(6) nnn since the Al(6) nnn causes an increase in the average Al—O bond length, enhancing the shielding [100]. $Q^n$ species are poorly distinguished by $\delta_{iso}$ which is attributed to the relative similarities of Al—O bridging and non-bridging bonds as compared to Si—O and P—O.

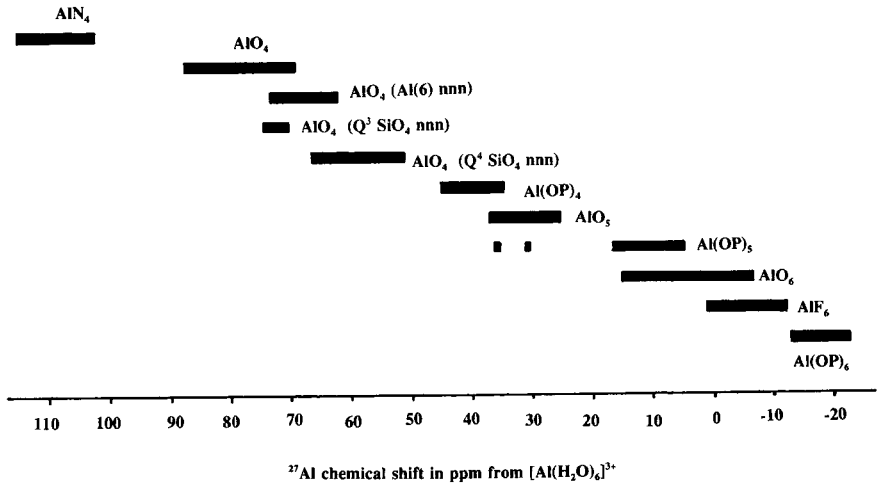


**Fig. 16.** $^{27}$Al isotropic chemical shift ranges of different coordinations in solids.

For Al(6) units an early study suggested that $\delta_{iso}$ showed large changes with increasing bond covalency through the sequence: isolated, corner-sharing, edge-sharing to face-sharing. The veracity of the suggestion is difficult to ascertain as the experiment was performed at low field and the suggestion based on uncorrected peak positions [5]. For Al(4) $C_q$ and $\eta$ are more sensitive to changes in site symmetry than $\delta_{iso}$ with $Q^1$ and $Q^3$ generally giving $\eta \sim 0$ and $C_q(Q^0,Q^4) < C_q(Q^1,Q^2,Q^3)$. Systems studied include $Li_2O$-$Al_2O_3$ [10], CaO-$Al_2O_3$-$H_2O$ [58, 101, 102], BaO-$Al_2O_3$-$H_2O$ [103], $Y_2O_3$-$Al_2O_3$ [73], $La_2O_3$-$Al_2O_3$ [104] and CaO-$(Eu,La,Y,Pr)_2O_3$-$Al_2O_3$ [105]. $Y_4Al_2O_9$ contains isolated $(Al_2O_7)^{6-}$ groups with two Al(4) connected via a single bridging oxygen and for this unit $C_q$ must be very large as no Al(4) resonance could be observed under MAS. However a prominent Al(6) resonance was seen that could be attributed to a very minor impurity (< 2%) of $YAlO_3$ that could not be detected by XRD illustrating that $^{27}$Al MAS NMR is good at characterizing very minor components in phase mixtures [73]. Measurement of the phonon-impurity relaxation time in the solid solution $Y_{3-x}Lu_xAl_5O_{12}$ showed an anomalous peak at $x \sim 0.75$, the same composition that gave the minimum $^{27}$Al NMR linewidth, suggestive of Y/Lu ordering [106]. Recently some impressive experiments involving in-situ melting of aluminates, requiring temperatures up to 2110°C, using a laser heated levitation NMR probe have been performed which show that $LaAlO_3$ (74 ppm), $YAlO_3$ (71 ppm), $Y_3Al_5O_{12}$ (68 ppm) and α-$Al_2O_3$ (53 ppm) appear to become Al(4) in the molten state compared to being predominantly Al(6) in the solid [107]. Al(5) containing crystalline phases are quite rare but the resonances have been reported from barium aluminium glycolate ($BaAlO_8C_{6.75}H_{14.75}$) [60, 61], $Al_2Ge_2O_7$ and $LaAlGe_2O_7$ [26].

Dehydration of $Na_2O \cdot Al_2O_3 \cdot 3H_2O$ was followed by $^{27}Al$ NMR in the temperature range (100–600)°C with the changes generally reflecting the water content. The Al(4) unit in the sodium form gives $\eta \sim 0.85$ compared to $\sim 0$ for the potassium form [108], indicating the differences in the Al(4) coordinations in these two compounds of $Al(OH)_2(OAl)_2$ and $Al(OH)(OAl)_3$ respectively. The fully hydrated forms are polymerized with Al–O–Al linkages but the NMR evidence cannot distinguish cyclic or linear possibilities. Dehydration produces a decrease in $C_q$ as $Q^0$ units form taking only 10 minutes to complete at 400°C but more than 1000 minutes at 150°C [108].

The cation ordering in $AB_2O_4$ spinels over the tetrahedral and octahedral interstitial sites in the oxygen lattice range from $A(4)B(6)_2$ in a normal spinel to B(4)A(6)B(6) in the inverse case. For stoichiometric spinel ($MgAl_2O_4$), natural samples tend to have a lower degree of inversion (i.e. B(4)/B(6)) than synthetic samples, for which a maximum inversion of 0.4 was found in samples quenched from 900°C and above [109, 110]. This inversion has profound consequences for the thermodynamics of some important geomineral reactions. A solid solution $MgO \cdot xAl_2O_3$ $(0 > x > 3.5)$ exists at elevated temperatures where $Mg^{2+}$ is replaced by $Al^{3+}$ and charge balancing vacancies. The increase of Al(4) content with $x$ was followed readily by MAS NMR and under the assumption that no magnesium inversion occurs, preferential occupation of the octahedral sites is suggested [111]. Subsequent re-examination of the data allowing for some magnesium inversion shows that this scheme cannot be distinguished from a random distribution but there is clearly no preference of the vacancies for the tetrahedral site [112]. Much more accurate Al(4)/Al(6) ratios could now be obtained by employing faster MAS.

Calcium aluminates and their hydrates have been extensively studied because of the role they play in the chemistry of cements [113, 114]. Of particular note in $CaAl_6O_{10}$ the two Al(6) sites could be distinguished but the Al(5) site could not be observed and in $CaAl_4O_7$ the large $C_q$ was attributed to some oxygen sites being tri-coordinate [101]. In hydration of calcium aluminates there is a coordination change Al(4) to Al(6). The process has three stages: an initial induction period, then rapid Al(4) to Al(6) conversion followed by a slower conversion regime [113]. NMR showed that the actual phases formed and their rate of formation markedly changed between 70°C and 20°C with the reaction rate slowing by two orders of magnitude. The addition of lithium-containing accelerators was shown not to increase the rate of reaction but simply to remove the induction period as initially precipitated hydrated $LiAlO_2$ overcame the nucleation barrier [115].

A combination of single crystal and powder MAS NMR of $^{27}Al$ in rutile ($TiO_2$) revealed the aluminium dissolution mechanism. The single crystal work showed two sharp resonances on top of a broader one, the latter corresponding to an exsolved phase that is reduced on heating to 1500°C. The two narrower lines reveal aluminium nuclei experience little dipolar

coupling, which together with only two distinct sites indicate that aluminium replaces titanium rather than being on interstitial octahedral positions as there would then be four resonances [116]. Dehydration and calcination of Al-Nb-O sols gives a largely amorphous catalyst support between (500–750)°C with three peaks at 58, 30 and 0.8 ppm. Above 750°C $AlNbO_4$ crystallizes out [117]. Arsenoaluminates $AlAsO_4$-5 and $AlAsO_4$-6 can be formed hydrothermally using ethylenediamine as a template molecule give resonances at − 14.5 and − 8 ppm respectively, as compared to fully dense $AlAsO_4$ at 47 ppm [118].

## 6. Zeolites

Understanding the aluminium ordering and changes that occur on dealumination in the commercially important zeolite catalysts provided much of the early impetus for solid state $^{27}$Al NMR. These microcrystalline compounds of general formula $M_{x/n}(AlO_2)_x\,(SiO_2)_y \cdot mH_2O$ ($y > x$) are difficult to characterize by conventional XRD experiments due to similarity in the X-ray scattering factors of silicon and aluminium and their microcrystalline nature. The acid sites of the zeolite structure are associated with framework aluminium so that its aluminium content and distribution are key materials properties. Dealumination can be used to control these properties, but detailed understanding of the structural changes that occur are largely limited by the amorphous nature of the non-framework species. Previous reviews have covered the early development of the subject [99, 119–121].

Al(4) sites in aluminosilicate frameworks give resonances in the range (51.5–65) ppm below the values associated with aluminates (Fig. 16, Table 4) [119]. The distortion of the Al(4) site is strongly linked to the counter ion and the degree of hydration. For zeolite rho the anhydrous form produces a highly distorted site but sorption of water or methanol restores the symmetry [122, 123]. Dehydration of $NH_4$-ZSM5 increases $C_q$ from 0.85 MHz to 1.97 MHz after 3 days at 503 K. However the loss of intensity of the spinning sidebands from the non-central transitions is more pronounced due to a reduction in the correlation time of the molecular motion in the cage. This moves the system from the fast exchange limit to the intermediate regime which interferes with the formation of the rotational echoes [72]. The $^{27}$Al relaxation time increases markedly on dehydration from ~ 1 ms to > 100 ms in zeolite A as the motion of the sorbate molecules decrease. This reduces the modulation of $C_q$ at the aluminium site which has been shown for zeolites to be the dominant relaxation mechanism [124]. The aluminium signal from the framework can be observed even in highly siliceous materials where (Si/Al) ~ 1000. However the ability to resolve crystallographically distinct sites is limited compared to $^{29}$Si as a result of the smaller range of isotropic chemical shifts and broader MAS NMR resonances for $^{27}$Al. In-

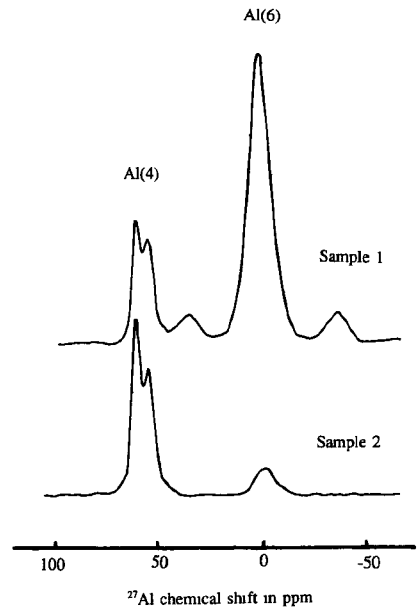


**Fig. 17.** 9.4 T $^{27}$Al MAS NMR spectrum of zeolite Ω formed from kaolinite showing two tetrahedral sites and the original kaolinite after 50% conversion (sample 1) and 90% conversion (sample 2). (From [129] with permission of the Royal Society of Chemistry.)

stances of the detection of inequivalent aluminium sites do exist, including ZSM-5 [125, 126] and mazzite (zeolite Ω) [127–130], which has two Al(4) sites (Fig. 17). Zeolite Ω has four-membered and six-membered rings with tetrahedral sites in the ratio 2 : 1. Conversion of kaolinite into zeolite Ω showed that the ratio of these two peaks in the NMR spectrum changes from 1.10 : 1 to 1.26 : 1. This demonstrates that the aluminium occupation is non-random and favours the six-membered rings, which is more pronounced during the early stages of formation so that distributional zoning of the aluminium occurs [129].

Extensive studies of zeolite dealumination have been reported including zeolite A [131, 132], zeolite Y [133–143] and zeolite Ω [128, 130]. Commonly either steam or $SiCl_4$ are used to remove aluminium from the framework, which decreases the activity of the zeolite decreasing problems of coking and promoting the thermal stability of the zeolite, and is referred to as ultrastabilization. In this process, aluminium is ejected from the actual framework but remains as a largely amorphous species within the pore space, much of which can be subsequently leached out. It was established that on expulsion from the framework the aluminium coordination changes from four to six (Fig. 18) [e.g. 144]. A major problem was the inability to reconcile the aluminium distribution indicated by NMR spectra and that known to be present from chemical analysis (i.e. inconsistent amounts of

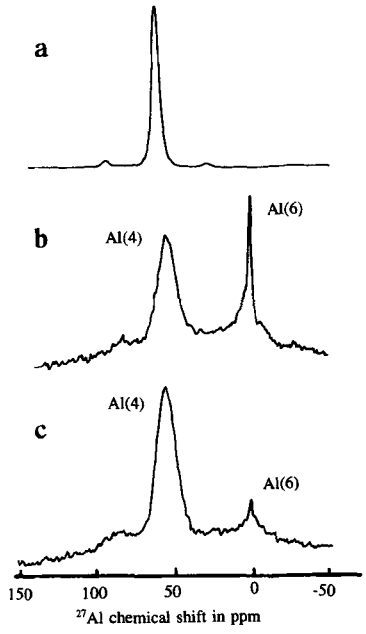


Fig. 18. 9.4 T $^{27}$Al MAS NMR spectra showing the dealumination of NaY-zeolite **a** intially, **b** after heating at 560°C with $SiCl_4$ for 3 hours and washing with distilled water and **c** after extensive washing. (Reprinted with permission from [144] copyright 1983 the American Chemical Society.)

Al(6) knowing the framework composition). The missing aluminium was known as "NMR invisible" aluminium, being attributed to sites with large $C_q$. In $^{27}$Al spectra of dealuminated samples, broad underlying peaks could be observed [145]. Addition of complexing agents such as acetyl acetone often increased the amount of observed aluminium as $C_q$ at some sites were reduced [146]. Much work was done on zeolite Y and understanding of the spectrum has improved with the technique. Work at 11.7 T showed three peaks at ~ 60, 30 and 0 ppm [135]. Nutation spectroscopy revealed distorted Al(6) sites (i.e. large $C_q$) and Al(4) sites with a range of $C_q$. Important questions were whether the distorted Al(4) was part of the framework or not and what was the origin of the 30 ppm peak? One interpretation of the 30 ppm peak was as the low frequency part of a very distorted Al(4) site [135]. It was however suggested that on steaming zeolites Al(5) species often formed [147]. Later fast MAS combined with observation at more than one magnetic field showed that this was so (Fig. 19) [83]. CP experiments revealed the 0, 30 ppm and part of the 60 ppm lines cross-polarized strongly to $^1$H and that these signals could be attributed to Al(6), Al(5) and Al(4) in an amorphous aluminosilicate phase, since very similar spectra could be produced by steaming silica-alumina mixtures (Fig. 19) [83, 84].

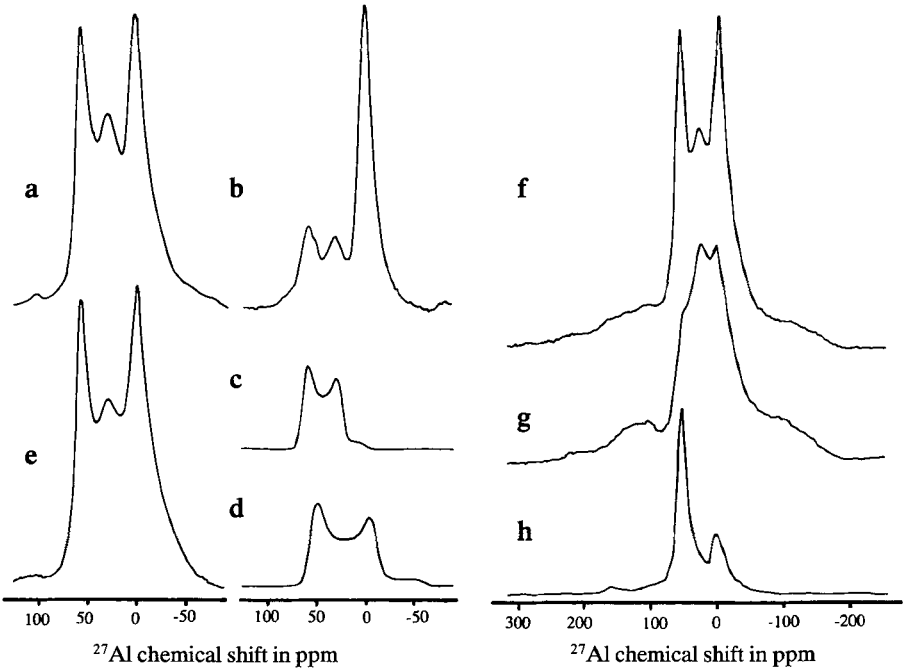


**Fig. 19.** $^{27}$Al MAS NMR spectra of NaY-zeolite after a double ammonium exchange and an aluminium exchange followed by calcining at 650°C, 1 atm of steam 2 h in a 20 cm deep bed **a** at 9.4 T, **b** with $^{1}$H CP. A simulation of the suggested Al(4) at **c** 9.4 T and **d** 7.1 T and **e** 7.1 T spectrum are also shown. A comparison of the 7.1 T $^{27}$Al MAS NMR spectra of **f** steamed NaY-zeolite with a silica-alumina mixture **h** prior to heat treatment and **g** after an identical steaming. (From [83] with permission of Elsevier Science Publishers.).

## 7. Framework Aluminosilicate Minerals

Framework aluminosilicate minerals provide a rich source of often structurally well characterized compounds, some with unusual coordinations, such as Al(5) in andalusite. Extensive $^{27}$Al NMR work has been performed on these systems and reviewed [148, 149]. Early single crystal work determined $C_q$ and $\eta$ in a number of cases [150]. The magnitude of $C_q$ has been correlated to parameters that reflect the distortion of the local coordination polyhedra, such as the longitudinal strain ($= \sum_i |\ln(l_i - l_o)|$ where $l_i$ is the individual Al—O bond length and $l_o$ is the bondlength corresponding to an ideal octahedron with the same volume) and the shear strain ($= \sum_i |\tan(\vartheta_i - \vartheta_{ideal})|$, where $\vartheta$ is the O—Al—O bond angle) [144]. Careful extraction of $\delta_{iso}$ for $^{27}$Al has shown that, as for silicon, it is sensitive to nnn effects, bond lengths and bond angles, the latter giving a correlation [30]:

$$\delta_{is}(\mathrm{Al}) = -0.5\,\vartheta + 132\ (\mathrm{ppm})\,. \tag{23}$$

As for zeolites the resolution is usually insufficient to reveal crystallographically distinct sites, although nepheline and leucite are exceptions [28, 30]. Mullite, a poorly crystalline aluminosilicate of general composition $Al_{4+2x}Si_{2-2x}O_{10-x}\square_x$ ($\square$ = vacancy) also shows two distinct Al(4) sites at ~ 69 and 42 ppm in addition to an Al(6) signal. The 42 ppm peak is thought to be from Al(4) with tri-coordinate nn oxygens [151]. Formation of mullite via colloidal, polymeric and spray pyrolysis methods proceeds by differing atomic arrangements. The early stages all show Al(4) and Al(6), with additionally Al(5) in small amounts by the polymeric route and large amounts for spray pyrolysis. The amount of Al(5) can be correlated with the size of the 980°C exotherm and the subsequent formation of $\gamma$-$Al_2O_3$ initially in the colloidal and polymeric preparations compared to the direct formation of a 3 : 2 mullite from the amorphous state in spray pyrolysis [152].

The elemental Si, Al disorder is of significance to the thermodynamic equilibrium of minerals as it influences the entropy of the system. Lowenstein's rule prevents Al—O—Al linkages [148] so that only $Al(OSi)_4$ units occur. Increasing Si, Al disorder tends to cause increasing NMR linewidths due to the increase in the range of bond lengths and angles. In alkali feldspars the $^{27}$Al NMR linewidth of the intermediate (Na, K)-compositions is greater than the end members of the series due to disorder in the (Na, K) distribution [153, 154]. For sodic feldspars increasing time at elevated temperatures causes increases in the $^{27}$Al linewidths due to disordering of the sodium [155]. Disordering effects have also been observed in the scapolite series ($Na_4Al_3Si_9O_{24}Cl$-$Ca_4Al_6Si_6O_{24}CO_3$) [156] and in the series pyrope ($Mg_3Al_2Si_3O_{12}$)-majorite ($Mg_4Si_4O_{12}$) [157] where cation disorder only occurs over the octahedral sites as only Al(6) is observed throughout. Although $^{29}$Si is more sensitive to differing sites, studies of leucite proposed widely different ordering schemes because the complex $^{29}$Si spectra were difficult to unambiguously interpret. $^{27}$Al spectra constrained this interpretation as the three distinct tetrahedral sites could be resolved with T1, T2 and T3 assigned to $\delta_{iso}$ 69.2, 64.7 and 61.0 ppm respectively on the basis of a $\delta_{iso}$-bond angle correlation similar to Eq.(23), as their mean bond angles are 145.9°, 138.9° and 130.4°. The aluminium distribution obtained directly from the $^{27}$Al spectrum disagreed with those required by the previous assignments of the $^{29}$Si spectra which consequently led to the $^{29}$Si spectrum being reinterpreted. The element specificity of NMR means that rather than seeing effects averaged over all T—O—T′ bond angles, as with XRD, the bond angles associated with the particular sites probed are observed. In disordered phases the $^{27}$Al resonances appear to higher frequency than expected from the mean bond angle so that aluminium must be associated with sites with the larger bond angles [28]. Further work in this area would be of much interest.

## 8. Layer Aluminosilicates

Layer aluminosilicates are important constituents of clay minerals and soils, and are precursors to a number of catalysts and ceramics. They consist of a series of separate tetrahedrally and octahedrally coordinated layers, the latter of which contain either magnesium (trioctahedral) or a mixture of aluminium and vacancies (dioctahedral) (Fig. 20a), and are often poorly crystalline. Aluminium can occur as Al(6) (Fig. 20b), substitutionally as Al(4) (Fig. 20d) or in both (Fig. 20c) [7, 70, 158–163]. Previous structural characterization involved a combination of XRD (which can be difficult to interpret) with the silicon and aluminium distributed over the idealized structure with the overall (Si/Al) ratio determined by chemical analysis. $^{29}$Si NMR gives an accurate measure of the aluminium content of the tetrahedral layers but early $^{27}$Al NMR work found large discrepancies in the Al(4)/Al(6) ratios determined via NMR and that known from other techniques. This problem has largely been resolved by performing experiments at higher $B_0$ with fast MAS [70]. Both $\delta_{iso}$ and $C_q$ increase with decreasing Si/(Si + Al) and

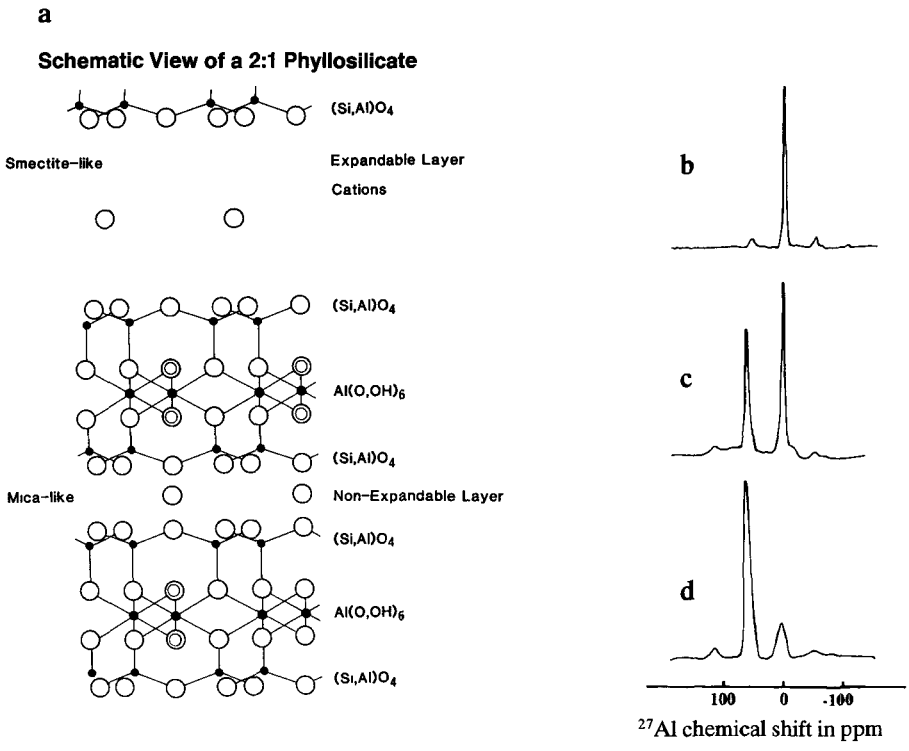


**Fig. 20.** **a** Idealized structure of a 2 : 1 phyllosilicate and $^{27}$Al MAS NMR spectra of clay minerals recorded at 7.01 T of **b** pyrophyllite, **c** muscovite and **d** phlogopite P8. (**b–d** reprinted with permission from [7] copyright 1984 American Chemical Society.)

with the total layer charge; properties which are related to increasing distortion of the layer. Correlations to these properties have been strong enough that the NMR parameters can be used to estimate them. The shift ranges from layer aluminosilicates is relatively small being (7.5–4.2) ppm for Al(6) and (70.5–74.5) ppm for Al(4). The Si, Al ordering within the tetrahedral layers has been shown to be much stronger than Lowenstein's rule and is such so as to minimize the number of Al–O–Si–O–Al linkages [e.g. 8].

Such minerals, together with materials such as imogolite and allophanes, are important constituents of soils [164]. These phases can be formed from spherical aluminosilicate particles. NMR of synthetic (8–10) nm hollow aluminosilicate spheres showed that the wall was similar to a 1 : 1 layer aluminosilicate with the tetrahedral and octahedral layers on the outside and inside respectively. Furthermore high levels (> 25%) of aluminium substitution in the Si(4) were observed together with high levels of defects in the Al(6) layer [165]. Weathering produces structural changes in already poorly-ordered aluminosilicates. Precipitation of such phases from solution shows that at Si,Al > 1 protoimogolite can form as well as disordered allophanes and the major aluminium coordination changes from Al(4) to Al(6). In such materials the combination of $^{29}$Si and $^{27}$Al NMR reveals that aluminium preferentially coordinates silicons that do not already have three aluminium nnn [166]. Structural transformation of layer aluminosilicates can result in highly complex intermediate states such as the 1.4 nm mineral appearing in Korean Utlisols, which is probably a result of conversion of muscovite to vermiculite and kaolin group minerals. The NMR data suggests that as this process occurs a 1 : 1 aluminosilicate forms in the interlayer space of the 2 : 1 parent compound [167]. Changes of structure in processes such as metamorphism and diagenesis, where smectite layers are converted to illite, are accompanied by changes in the Al(4) content, but again resolution of different Al(4) is poor [158, 168]. In rectorite both swelling (i.e. smectite-like) and non-swelling (i.e. mica-like) layers are present which from $^{29}$Si NMR have quite different (Si/Al) ratios, but only one Al(4) resonance is detected [8]. Generally the peaks in these materials do not show any second-order quadrupolar structure but tend to be skewed to negative shift indicating a range of $C_q$ and $\eta$. This spread is unsurprising given that there is a large degree of disorder with faults in the layer stacking, finite crystallite size and compositional disorder including aluminium/vacancy over the Al(6) sites. Halloysite and dickite have differing degrees of order according to XRD but give similar $^{29}$Si and $^{27}$Al NMR spectra suggesting that over the short-range they are similarly ordered [160]. Studying clays with varying iron-content has indicated that the iron distribution is very inhomogeneous with some very iron-rich domains [82]. CP-experiments revealed that 3.3% of the aluminiums occur at fault edges that can act as Bronsted acid sites [82]. Tobermorites, 2 : 1 layer hydrated calcium silicates, exhibit cation selectivity. Aluminium can partially substitute for silicon and NMR reveals it to all be Al(4) with two cation exchange sites identified. If a mixture of

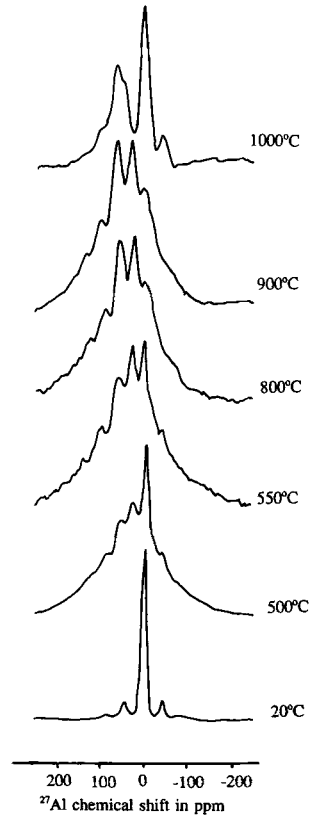


**Fig. 21.** $^{27}Al$ MAS NMR spectra at 9.4 T showing the thermal decomposition of kaolinite. (From [172] with permission of Springer Verlag.)

aluminium and sodium are substituted the sodium site can act as an additional exchange site. Then the cation selectivity changes from $Sr^{2+} < Ba^{2+} < Mg^{2+}$ to $Mg^{2+} < Sr^{2+} < Ba^{2+}$ [169].

One of the most important reactions in ceramic processing is the thermal decomposition of clay minerals. Various stages are involved with, initially, loss of hydroxyls from the Al(6) layer, then gross breakdown of the structure followed by phase separation into largely amorphous components that then chrysalises into phases determined by the initial composition. The intermediate dehydroxylate can vary between being crystalline for pyrophyllite to amorphous for kaolinite. Thermal decomposition of kaolinite has been extensively studied by MAS NMR [9, 170–176] but much of the early work was done at low fields (e.g. 4.7 T) and with slow spinning speeds (e.g. 3 kHz) so that as little as 10% of the total aluminium content was observed in the NMR spectrum [9]. Again, this has now been improved upon. For the intermediate metakaolinite phase it is clear that Al(4), Al(5) and Al(6) are

all present (Fig. 21) [174, 175]. At this stage simple rehydration will reverse the process [177]. Acid-leaching will preferentially remove the Al(5) [174]. (Note that extensive grinding of kaolinite has been shown to induce changes from crystalline to non-crystalline components, with Al(5) peaks forming, but annealing will again reverse the process [178]). Further heating will cause an irreversible structural breakdown and the Al(6) content reaches a minimum at around (750–800)°C, increasing again at higher temperatures [175]. Phase separation into silicon-rich and aluminium-rich phases occurs with some debate as to whether the aluminium-rich phase is $\gamma$-$Al_2O_3$ or a mullite phase. The inorganic fraction present in coals is largely kaolinite-like and on combustion of the coal this fraction shows similar structural changes as those observed for pure kaolinite [179]. Thermal decomposition of other systems has been studied. Pyrophyllite dehydroxylate has been shown to have a well defined Al(5) environment from XRD and from the 14.1 T NMR spectrum, which was fitted to a quadrupolar lineshape [180] but field dependent simulations have pointed out some discrepancies [58]. Other systems studied include pyrophyllite [181], montmorillonite [182], muscovite [183], imogolite [184, 185], polygarskite/sepiolite [186] and laponite [187] have been reported. The transformation in the pillaring of clays has also been followed [188–190].

## 9. Aluminosilicate Glasses, Gels and Fibres

Aluminosilicate glass structures are of significant technological interest and also serve as models for geological melts. Glasses from the binary $Al_2O_3$-$SiO_2$ up to 50 wt% $Al_2O_3$ have been studied with NMR and phase separation into Al-rich and Al-poor phases occurs between (15–40) wt% $Al_2O_3$. Roller-quenched specimens show three peaks that were attributed to Al(4), Al(5) and Al(6) [191]. An extensive study of aluminosilicate glasses showed that at quench rates of $(10^2–10^3)°C \cdot s^{-1}$ only Al(4) and Al(6) were present with the Al(6) content increasing with the level of aluminium. Glasses quenched at $(10^5–10^6)°C \cdot s^{-1}$ showed a broad underlying resonance and partially resolved peaks at 8, 27 and 55 ppm, which were assigned to Al(6), Al(5) and Al(4) (Fig. 22) [71]. From the slower quenched glasses all the aluminium was observed in the NMR spectrum, whereas those glasses that were more rapidly quenched were missing about (15–30)% of the aluminium, suggesting a much more distorted framework. It is believed that the $AlO_4^-$ of the framework is charge-balanced by the higher coordination species. Studies at more than one magnetic field showed that for Al(4) and Al(5) in the rapidly quenched glasses $C_q \sim 3.5$ MHz [71]. The changes of structure with quench rate indicate that extrapolation to the melt could be hazardous. Gel-derived aluminosilicate glasses show a more pronounced tendency to phase separate. On heating gels Al(4) is converted to Al(5) and

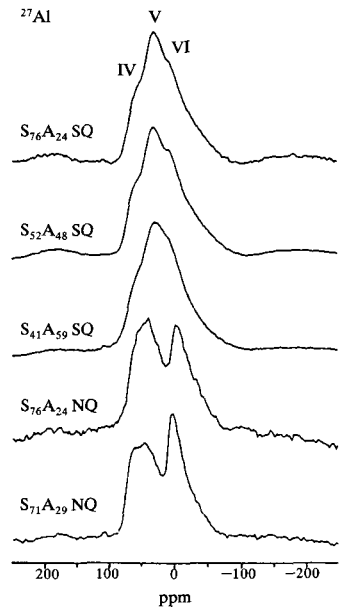


**Fig. 22.** $^{27}$Al MAS NMR spectra at 8.45 T with $\nu_r \sim 15$ kHz of rapidly quenched (SQ) and more slowly quenched (NQ) glasses of silica(S)-alumina(A) mixtures. (Reprinted with permission from [71] copyright 1991 American Chemical Society.)

Al(6), and as the full density is approached the Al(5) content begins to fall. The Al(4)/Al(6) distribution was observed to be different in gel-derived and melt quenched glasses but crystallization resulted in the same final phases [192].

In ternary systems $MO\text{-}Al_2O_3\text{-}SiO_2$ the aluminium coordination is the key to understanding the polymerization of the aluminosilicate framework [74, 75, 193–202]. In the system $SiO_2\text{-}CaAl_2SiO_6$ the glasses appear to be fully polymerized with no Al(6). A shift to more positive values is observed with decreasing Si/(Si + Al) which can be speculatively related to a decrease in the average number tetrahedra per ring although it should be recognized that NMR is poor at constraining intermediate range-order [75]. A lot of work has been done on the system $CaO\text{-}Al_2O_3\text{-}SiO_2$ and aluminium does not appear to act as a network modifier. For $CaO : Al_2O_3 = 1 : 1$ a fully polymerized network is present with $Ca^{2+}$ charge-balancing the framework $AlO_4^-$. When $Al_2O_3$ exceeds CaO higher aluminium coordinations form [74]. Aluminium tends to occupy the most polymerized part of the network but for CaO and MgO containing systems there is some evidence for aluminium occupation of $Q^3$ sites at high alumina content. This is also the case for $CaMgSi_3O_6\text{-}CaAl_2SiO_6$ with the peak tending to become more positive at higher alumina levels [196]. Jadeite glasses showed only Al(4) despite the crystalline compounds being exclusively Al(6) [197].

Changes of glass structure under differing physical conditions and on chemical reaction are also of interest. Albite ($NaAlSi_3O_8$) is often taken as a model aluminosilicate glass. Quenching a melt from 30 kbar and 1200°C only shows Al(4), but above 30 kbar increasing Al(6) content is revealed as the structure changes to relieve the pressure [199]. A more recent study at (8–10) GPa did not observe the narrow – 16 ppm peak of Ohtani *et al.* but with increasing pressure there was increasing intensity negatively shifted from the dominant Al(4) peak, consistent with increased aluminium coordination at some sites [200]. Hydrothermal reaction of glassy aluminosilicates at moderate temperatures (~ 250°C) is a common crustal process. Studies of albite [201] and rhyolite [202] showed that the secondary phases that formed varied with pH. Rhyolitic glass gave kaolinite and the original glass at pH < 3, whereas for pH > 9.1 the glass becomes hydrated (although not depolymerized) and an expandable smectite forms [202]. The reaction proceeds via a dissolution/precipitation mechanism. For an albite glass kaolinite forms at low pH, while for pH ~ 5 the secondary phase was an amorphous 2 : 1 phyllosilicate. At pH > 9 no Al(6) was found in the secondary phase which were p-zeolite and an amorphous aluminosilicate. Dissolution was again thought to proceed via a surface reaction [201]. Forcing water into an albite melt at high pressure and then quenching surprisingly caused no network depolymerization although the $^{27}$Al NMR linewidth did decrease with increasing water content indicating a reduction in $C_q$ [203]. Addition of CaO, $Li_2O$, BaO and SrO to synthetic albite glasses induced ordering of the glass, and, at > 80 mol% CaO caused crystallization and phase separation [204].

Amorphous gels prepared from solution are being increasingly used as precursors in low temperature synthesis routes for glasses [192, 205–212], and zeolites [213]. The ability of NMR to act as a local probe has allowed new insights to be gained into these amorphous phases and the structural changes that occur. On gelation polymeric chains tend to form, which on dehydration and heat treatment become three-dimensional frameworks. In aluminosilicate gels Al(4) tends to be dominant until (Si/Al) > 0.9 [205]. Addition of alkaline-earth cations shows a sharp increase in Al(4)/Al(6), as in the cation poor system the Al(6) species act as charge-balancers. The starting compositions influence the final phase-separation, with for example a mixture of sodium silicate and aluminate giving little Al(6) while gels formed from di-s-butoxyaluminooxytriethoxysilane have Al(4), Al(5) and Al(6) [211]. Similarly for cordierite prepared from a gel; initially a mixture of all three coordinations is observed with the higher coordinations converted to Al(4) on heating [208]. $^{27}$Al NMR of $Al_2O_3$-$SiO_2$ xerogels in the compositional range (21–73) wt% $Al_2O_3$ show that at high alumina content Al(6) is the dominant coordination, whereas at 21 wt% comparable amounts of Al(4) and Al(6) were observed. At all compositions Al(4), Al(5) and Al(6) exist. At 47 wt% $Al_2O_3$ the surface area decreases anomalously by about two orders of magnitude. No corresponding change is observed in the NMR spectrum in-

dicating that these effects must be on a scale larger than nnn [214]. The aluminosilicate fibre Nextel has a largely disordered structure but gives a clear NMR spectrum, similar to poorly crystalline mullite with an Al(6) site and two Al(4) sites [215].

## 10. Aluminophosphates

Systems containing Al–O–P linkages have found a number of applications including bioglasses and molecular sieves. The polymorphs of $AlPO_4$ are completely connected corner-sharing tetrahedral frameworks with strictly alternating Al(4) and P(4) that are isostructural to the polymorphs of $SiO_2$. A similar correlation of $\delta_{iso}$ of $^{27}Al$ with Al–O–P bond angle as for $^{29}Si$ in $SiO_2$ exists [216]. Metavariscite ($AlPO_4 \cdot 2H_2O$) has a well defined Al(6) coordination [217] while ammonium and alkali phosphates have both Al(4) and Al(6) coordinations [218]. For compounds with phosphorus nnn the $^{27}Al$ shift ranges associated with Al(4) and Al(6) are typically (25–35) ppm below the shift ranges associated with aluminates (Fig. 16). This shift is associated with the phosphorus decreasing the p-character of the Al–O bond. The aluminophosphate minerals senegalite and augelite have Al(5) (as well as Al(6)) environments with phosphorus nnn but their $\delta_{iso}$ of 36 and 31 ppm are very similar to Al(5) in aluminas and aluminosilicates (Table 4) [219]. The layer aluminophosphate tarankite ($H_6K_3Al_3(PO_4)_8 \cdot nH_2O$) was shown to contain all the aluminium as Al(6) [220]. In orientationally disordered $Na_3PO_4$ the substitution $Al^{3+} + 2\square \longleftrightarrow 3Na^+$ occurs with the aluminium going into an Al(4) site and in combination with $^{31}P$ MAS NMR shows that the substitution minimizes the number of Al–O–P linkages per P(4) [221].

$AlPO_4$ molecular sieves are formed by the hydrothermal treatment of aluminophosphate gels in the presence of a template molecule which can remain in the structure or subsequently be removed by calcination to leave an open channel structure. To optimize their stability, performance and formation the structures and their changes with hydration need to be well understood. $^{27}Al$ MAS NMR has appeared on $AlPO_4$-5 [222, 223], -8 [224], -11 [216–217], -17 [217], -21 [62, 228, 229] and -25 [229]. $AlPO_4$-21 contains Al(5) with P nnn and they show the expected positive shift of the Al(5) species with both sites being at 15 ppm (Fig. 23, [62]). Most others $AlPO_4$s show prominent Al(4) peaks in the range (45–35) ppm and some smaller resonances in the Al(6) range of $-$ (15–25) ppm. CP experiments considerably enhance the latter signal and its intensity is reduced on heating under vacuum, indicating that the conversion of Al(6) to Al(4) is by loss of coordinated water molecules. Structural changes with hydration and examination of preferential sites for water coordination have provided the first application of DOR to $^{27}Al$ NMR [227, 229, 230]. $AlPO_4$-25 has two Al(4) sites in the ratio 2 : 1. Ex-

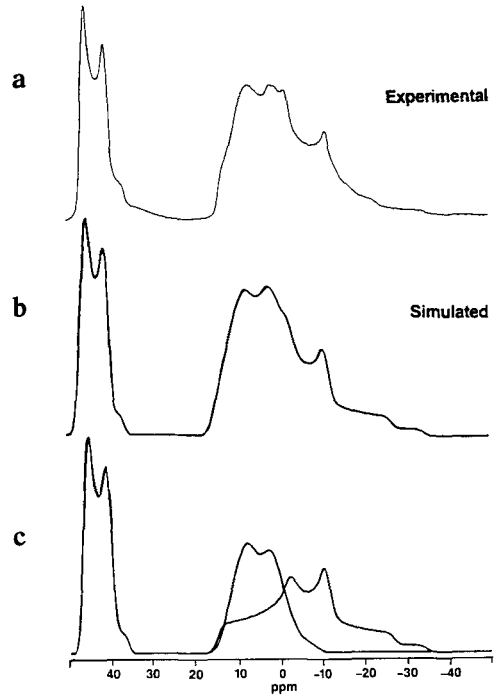


Fig. 23. **a** $^{27}$Al MAS NMR spectra of $AlPO_4$-21 at 11.7 T with $\nu_r = 13.2$ kHz with spectral simulations of **b** the complete spectrum and **c** the separate components. (From [62] with permission of Academic Press.)

periments at 11.7 T give no evidence for two sites, but studies at 4.7 T using DOR reveals two peaks at 21.9 and 33.6 ppm. The evolution of the spectrum with $B_0$ indicates that $\delta_{iso}$ are similar for the two sites but that their $C_q$ differ (Table 4). Hydration causes 25% of the sites to become Al(6) (Fig. 24, [229]). $AlPO_4$-11 contains channels made up of ten-membered rings and the body centred orthorhombic structure contains three crystallographically distinct Al, P(4) sites, but they cannot be distinguished by NMR [225–227]. On hydration, the structure becomes primitive orthorhombic and two Al(4) and an Al(6) site at $-18$ ppm were observed [225]. A later study at a higher magnetic field in combination with DOR showed three aluminium sites in the hydrated sample in the ratio 1 : 3 : 1, as well as the octahedral site and concluded that all the tetrahedral sites were equally susceptible to hydration [227]. VPI-5 is a remarkable aluminophosphate having 18-membered channels. The NMR spectrum consists of peaks at 40.7 and $-19$ ppm, the former splitting under DOR (Fig. 25, [230, 231]) to give three peaks in the ratio 1 : 1 : 1. The unambiguous assignment of these resonances to the 4- and 6-membered rings of the structure, as well as which sites hydrate is not possible on the basis of the NMR results, although following the hydration process reveals a large number of sites formed in the intermediate state (Fig. 25).

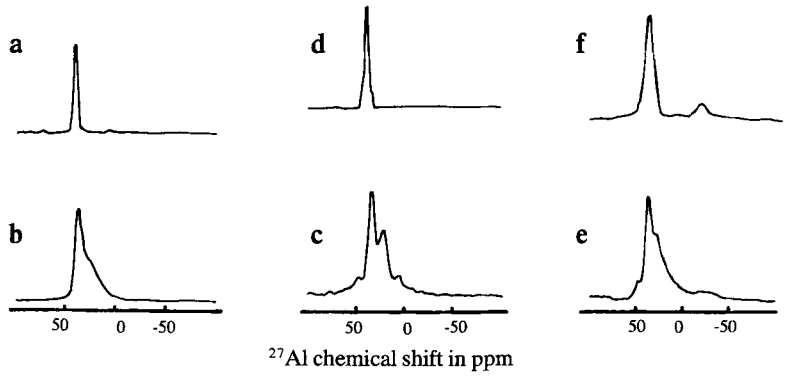


**Fig. 24.** $^{27}$Al MAS NMR at $\nu_r = 5.5$ kHz of dehydrated $AlPO_4$-25 at **a** 11.7 T and **b** 4.2 T and DOR spectra with the outer rotor at 750 Hz at **c** 11.7 T and **d** 4.2 T. $^{27}$Al DOR NMR spectra of hydrated $AlPO_4$-25 at **e** 11.7 T and **f** 4.2 T with the outer rotor spinning at 650 Hz (Reprinted with permission from [225] copyright 1991 American Chemical Society.)

NMR has shown in making $AlPO_4$ molecular sieves from aluminophosphate gels in the presence of template molecules that the framework structure forms during the early stages of the reaction [232]. However there is some

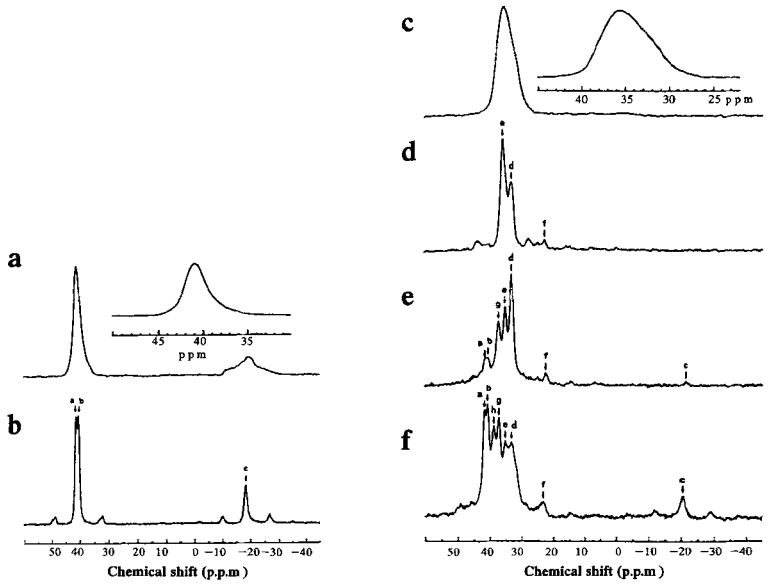


**Fig. 25.** $^{27}$Al NMR spectra of hydrated VPI-5 at 9.4 T using **a** simple MAS and **b** DOR (isotropic peaks are indicated by arrows) and **c** MAS and **d** DOR spectra of a dehydrated sample with **e** and **f** showing partial rehydration. (Taken with permission from Nature **346**, 550, copyright 1990 MacMillan Magazines Ltd.)

variability to the structure giving a spread of bond lengths and angles, and for the cases of $Pr_3N$-$AlPO_4$-5 gives a spread of $\pm 0.5$ MHz in $C_q$ [232]. The template molecule is thought to initially enhance the stability of the Al(4) site by physically preventing reaction with water to form Al(6). Reaction of phosphoric acid with pseudoboehmite gel converts Al(6) to Al(4). The absence of a template molecule allows reconversion to Al(6), so that Al(4) formation is favoured by high ($P_2O_5/Al_2O_3$) and ($Et_3N/Al_2O_3$) ratios [233]. Aluminophosphates formed from solutions with excess alumina (i.e. $P/Al < 1$) are largely amorphous and the question is at the local level do $Al_2O_3$ and $AlPO_4$ form as pure phases or does a continuous disordered lattice with aluminium and phosphorus distributed over it form? No linear combination of $\gamma$-$Al_2O_3$ and $AlPO_4$ spectra could reproduce the observed spectra which suggests a distribution of $Al(OAl)_n(OP)_{4-n}$, accounting for the very different properties of the mixture compared to the end-member phases [234].

Many elements can be substituted within the $AlPO_4$ framework; silicon is common forming SAPOs. Two substitutional mechanisms can be envisaged, either pairwise (P, Al), or preferential substitution of the phosphorus [228, 235–240]. It is unclear as to whether one is universally favoured, probably depending to some extent on the composition and formation conditions. Other substitutions studied include boron into $AlPO_4$-5 [241] and magnesium in the sodalite structured $AlPO_4$-20 [242]. For MgAlPO-20 the shift of 34.4 ppm is quite negative even for $Al(OP)_4$ units and is related to the large mean Al–O–P bond angles. Magnesium was shown to substitute exclusively on the aluminium sites and modeling the $^{31}$P spectral intensity distribution showed that the compound was atomically very ordered [242]. Manganese ($Mn^{2+}$) replaces aluminium in $AlPO_4$-5 and despite having an unpaired electron, $T_{1e}$ is sufficiently short that only moderate broadening occurs and the contact shift is small [243].

Glasses from the system $CaO$-$Al_2O_3$-$P_2O_5$ showed three peaks at $-21$, 4 and 37 ppm which were assigned to $Al(OP)_6$, $Al(OAl)_6$ and $Al(OP)_4$ [244]. Similar spectra were observed from alkali aluminophosphate glasses [245], $Sb_2O_3$-$Al_2O_3$-$P_2O_5$ [246] and the binary $Al_2O_3$-$P_2O_5$ [245] precluding cation effects being their source. Early work was hampered by loss of intensity with some samples showing as little as 20% of the total aluminium content [244].In the antimony system at high antimony contents a fourth resonance at (51–57) ppm became dominant [246]. More recent studies at higher magnetic fields have shown that in $xAl_2O_3 \cdot (1-x)NaPO_3$ for $x < 0.125$ Al(6) was dominant, but at higher alumina contents Al(4) becomes favoured [245]. The change in the coordination can be explained as Al(6) can satisfy oxygen's bonding requirement at low phosphorus content, but beyond the diphosphate composition (14.3 mol% $P_2O_5$) lower aluminium coordination are necessary to prevent oxygen from becoming underbonded [245]. The 4 ppm resonance (Fig. 26) was reassigned to $Al(OP)_5$ rather than $Al(OAl)_6$ on

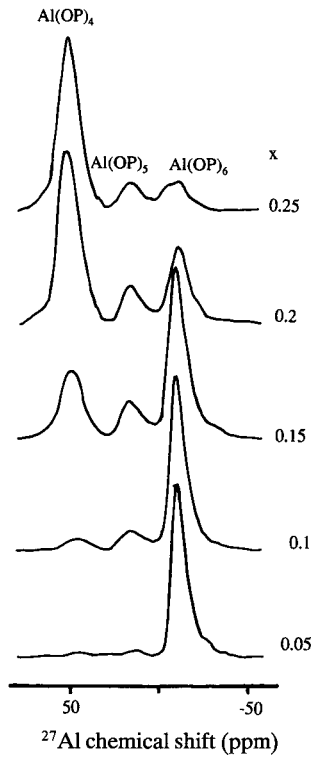


**Fig. 26.** $^{27}Al$ MAS NMR spectra of $xAl_2O_3 \cdot (1-x)NaPO_3$ glasses. (From local structure of $xAl_2O_3 \cdot (1-x)NaPO_3$ glasses: An NMR and XPS study, R.K. Brow *et al.* J. Am. Ceram. Soc. **73**, 2293 (1990) with permission of the American Ceramic Society.)

the basis that segregation into only all phosphorus or all aluminium nnn is unlikely unless phase separation occurs, for which there is no evidence [245]. In the $Al_2O_3$-$P_2O_5$ binary $T_g$ increases and the thermal expansion coefficient decreases with increasing aluminium content which is related to increasing cross-linking of the metaphosphate chains [245]. On conversion of Al(6) to Al(4) in these glasses there is a discontinuity in these properties, illustrating how probing the atomic level can aid understanding of bulk properties. The addition of phosphorus to alkali silicate glasses causes repolymerization of the silicate network such that at high phosphorus-content $SiO_6$ sites form in an amorphous $Si_2P_2O_7$-like phase. The introduction of aluminium to give a composition of $Na_2O \cdot 2SiO_2 \cdot (3-x)P_2O_5 \cdot xAl_2O_3$ reduces the intensity of $SiO_6$. This is thought to be due to preferential occupation of the octahedral sites by aluminium rather than any underlying structural change. At higher alumina-contents peaks at $-20$, 8 and (35–41) ppm are observed for $^{27}Al$. No change in the relative intensities of these lines occurs up to $x = 0.9$ but then progressive loss of Al(6) occurs up to $x = 1.5$ when Al(6) disappears. This is interpreted as changes in the relative stability of the amorphous structures [247].

## 11. Aluminoborates

Most interest in these materials has centred on glasses and glass-ceramics since they are potentially useful as sealing agents or as separators in environments where attack by alkali metals, such as batteries, is likely. All early work on alkali (and alkali-earth) aluminoborate glasses $M_{(2)}O$-$Al_2O_3$-$B_2O_3$ for Li [248], Na [248, 249], K [248], Mg [248, 250, 251], Sr [248, 251] and Ba [248, 251] was characterized by resonances near 0, 30 and 55 ppm. These works generally assigned the resonances as Al(6), Al(4) with B(3) (trigonal) nnn and Al(4) with Al or B(4) nnn. With differing quench rates of the $Na_2O$ glasses of 1 $K \cdot min^{-1}$ and $10^4$ $K \cdot min^{-1}$, samples with fictive temperatures that differ by around 100 K are produced, and the more rapidly quenched glass shows a 10% reduction in the $^{27}$Al signal intensity suggesting that this glass was more disordered [249]. Crystallization of MgO-$Al_2O_3$-$B_2O_3$ glasses showed structural changes but no $Al(OB)_6$ units form as in the phase $Al_{18}B_4O_{22}$ [250]. At different compositions in the system PbO-$Al_2O_3$-$B_2O_3$ four resonances were observed with the fourth one resonating at 78 ppm at high PbO content [248]. Studies of the dissolution mechanism of aluminium as either $\alpha$-$Al_2O_3$ or albite in fluxes of $2PbO \cdot B_2O_3$ in the range (1−23.8) mol% aluminium showed that the bulk of it enters as Al(4) with little dependence on the total aluminium content in this range. With $\alpha$-$Al_2O_3$ two other peaks appear at 0 ppm associated with Al(6) and a small peak (< 2%) at 30 ppm which is probably Al(5) and does not appear with albite [253]. For alkali aluminoborates as $SiO_2$ is added even at high silica contents Al(6) is present. This is very different behaviour from non-boron containing systems and it has been suggested that the B(4), B(3) equilibrium stabilizes that for Al(4), Al(5), Al(6) [251].

The original assignments of the $^{27}$Al spectra from alkali (earth) aluminoborate glasses has recently been questioned [251]. Electronegativity arguments cannot justify $Al(OB(4))_4$ and $Al(OB(3))_4$ being separated by as much as 25 ppm. It is also a little difficult to envisage $Al(OAl)_4$ and $Al(OB)_4$ appearing without any intermediates with mixed nnn, and 55 ppm is too negative for Al(4) with all aluminium nnn. The lack of observed mixed nnn species could be explained if they had large $C_q$ but this can be discounted as the crystalline phase $SrAlBO_4$ has $Al(OB)_2(OAl)_2$ and produces an observable resonance at 62 ppm [251]. Hence the middle peak is most likely Al(5) and changes in the peak position of the Al(4) with composition is as a result of changes in the average character of the nnn [251]. Studies at more than one magnetic field show that $C_q$ is only (1−2) MHz [251]. Although the main structural changes occur with composition some cation effects are noticeable; for example at 40 mol% MO magnesium gives 33% Al(4) while barium produces 75%. Hence the structures of these glasses are complex mixtures of B(3), B(4), Al(4), Al(5) and Al(6) governed by some subtle equilibria.

## 12. Fluorine-Containing Systems

A series of crystalline ammonium and alkali fluorides and their hydrates containing well defined $AlF_6$ units were investigated by $^{27}Al$ NMR. Their shift range was $0 - (-14)$ ppm and $\delta_{iso}$ was much less sensitive to structural changes than $C_q$ (Table 4). For isolated $(AlF6)^{3-}$ units $C_q$ is no larger than 1.5 MHz whereas for chains and layers these units are in the range (7.5–13.5) MHz [254]. Fluoroaluminophosphate glasses have attracted attention because of their favourable optical properties and good mechanical and chemical durability. Addition of fluorine to $Al(PO_4)_3$ as $BaF_2$ showed the formation of $AlF_6$ [255]. In the complex Ba-Al-P-O-F-(N) system three resonances were observed at $-9$, 13 and 50 ppm probably associated with Al(6), Al(5) and Al(4). As the fluorine content is increased the 13 and 50 ppm lines show a (3–4) ppm negative shift which could indicate that fluorine is bonding to these units at the same time as the proportion of

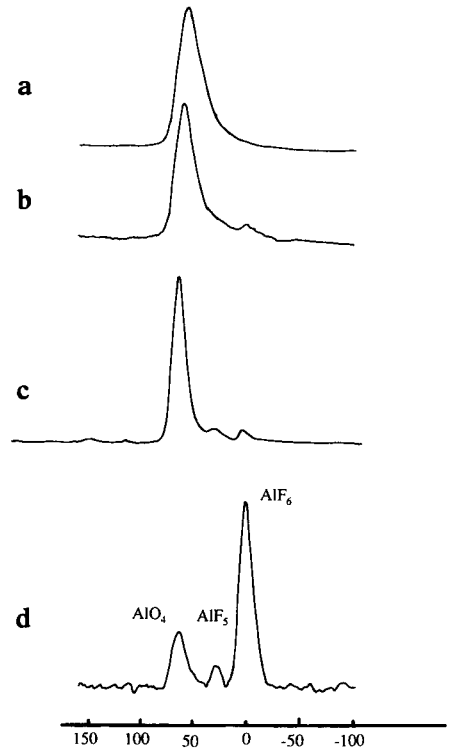


**Fig. 27.** $^{27}Al$ MAS NMR spectra of **a** jadeite glass and jadeite-NaF glass ($Na_3Al_2Si_4O_{12}F$) at **b** 8.45 T, **c** 14.1 T and at **d** 8.45 T with $19F$-$^{27}Al$ CP (Taken from NMR evidence for five- and six-coordinated aluminium fluoride complexes in F-bearing aluminosilicate glasses S.C. Kohn *et al.* Am. Mineral. **76**, 309 (1991) with permission of the American Mineralogical Society.)

$Al(OP)_6$ is increasing [255]. The effect of CaF additions to calcium aluminate glasses showed little effect on the $^{27}$Al NMR spectra despite the expectation that $AlO_3F$ units would be formed. The only observable difference was a very small (~ 1%) Al(6) peak at 9 ppm in the fluorine-free glass [256, 257].

$AlO_4(OH,F)_2$ units occur in minerals such as topaz (~ 3 ppm) and the series amblygonite ($LiAlPO_4F$)-montebrasite ($LiAlPO_4OH$) (~ − 10 ppm). The latter series contain two crystallographically distinct Al(6) sites but only one broad resonance is observed that shifts from − 11.3 ppm to − 8.7 ppm as F/(F + OH) changes from ~ 0.15 to 0.75 which was explained as a decrease in the bond covalency at the aluminium site [258]. Dissolution of fluorine in magmatic melts has marked effects on their physical properties, thought to be due to changes in the structure. Anhydrous jadeite glasses with additions of either NaF or cryolite were quenched from melts at 1250°C and (3−3.5) kbar. Experiments showed asymmetric lineshapes indicative of a range of $C_q$ and $\eta$. Al(4) is dominant (> 93.5%) at all compositions, but small Al(5) and Al(6) resonances are present which become clearer at higher applied magnetic fields (Fig. 27) [85]. $^{19}$F-$^{27}$Al CP experiments preferentially enhance the Al(5) and Al(6) resonances at short contact times, suggesting that $AlF_5$ and $AlF_6$ environments are present agreeing with the observed shifts [85]. Such units must be accompanied by the formation of non-bridging oxygens in the jadeite network which is consistent with the $^{29}$Si MAS NMR spectrum [85].

## 13. Metals and Semiconductors

Aluminium metal shows a Knight shift due to conduction electrons of 0.164% and a room temperature $T_1$ of 5 ms [259]. The static NMR lineshape of $^{27}$Al was seen to change in Cu-Zn-Al alloys on passing through the 152 K martensitic phase change, consistent with the local atomic rearrangement. The spectra were generally deconvoluted into two resonances with the lower temperature phase showing a Knight shift of (0.09−0.0975)%, larger than the higher temperature phase indicating an increased s-electron density. The lower temperature phase can be seen prior to 152 K with its proportion becoming dominant below the transition temperature [260].

Aluminium forms cubic compounds with the Group V elements P, As and Sb that have important semiconducting properties. The widths of these $^{27}$Al resonances are related to exchange effects. The spinning sideband envelopes are Lorentzian indicating that some sites experience efg due to point defects [261]. Successful predictions of the trend in $\delta_{iso}$ in these materials have been made using Harrison's bond-orbital method and the Szigeto effective charge $e_s^* = 3e_T^*(\varepsilon_\infty + 2)$, where $e_T^*$ is the effective transverse electronic charge and $\varepsilon_\infty$ is the high frequency dielectric constant [262].

For $Al_xGa_{1-x}As$ the aluminium bonding is poorly understood as it is dominated by changes in the conduction band. As $x$ goes from 1 to 0.25, the $^{27}Al$ NMR resonance shifts from 131 ppm to 136.5 ppm. So that as $x$ increases there is an effective decrease in the electron density at the aluminium nucleus. This corresponds to an increase in the ionicity of the Al—As bond. On doping with silicon or boron a broad resonance centred at 40 ppm also appears but no assignment was made [263].

## 14. Nitrides and Oxynitrides

AlN is a stable non-toxic strong ceramic with high thermal conductivity that has become increasingly used as a heat sink in high power electronics. It has a hexagonal wurtzite structure with an $AlN_4$ environment, indicated by the isotropic chemical shift of 114 ppm due to the increased p-character of Al—N bonds relative to Al—O [264—268]. Preparation is either by nitridation of metallic aluminium or $AlCl_3/Al_2O_3$, often with trace additives such as $Y_2O_3$. The presence of oxygen species can seriously effect the bulk properties of AlN and $AlO_6$ resonances can often be detected at trace levels (Fig. 1e). These oxygen environments can be emphasized by saturation of the $AlN_4$ resonance for which $T_1$ is (0.5—19) s depending on the paramagnetic ion content [266]. Ultrafine AlN powders react with water at room temperature producing $AlO_6$ at about 5 ppm [267]. The reaction is thought to proceed via some mixed oxygen/nitrogen nn environments but as they were not observed in the NMR spectrum it was suggested that these species react rapidly after their formation. However it is possible that the $C_q$ for such units may be large preventing their observation at moderate magnetic fields. The defect spinel structure of $\gamma$-$Al_2O_3$ can be stabilized at high temperature by the introduction of nitrogen. ALON phases form, centred around 33.7 mol% AlN. Usually three narrower peaks at 114, 65 and 12 ppm are seen on top of a much broader component [73]. Mixed nitrogen/oxygen environments should be present but it is only those species with either all nitrogen or all oxygen that narrow as the others have too large $C_q$ for the present spin rates and magnetic fields.

Ceramic alloying of nitride ceramics produces some high strength engineering materials. For example addition of silicon and oxygen to AlN form a series of layered polytypoid ($(Si,Al)_m(O,N)_{m+1}$) structures. To prevent any face-sharing by tetrahedra early NMR results showed that models predicting the formation of $AlO_6$ layers were correct even though only a small fraction of the aluminium sites gave narrow $AlO_6$ and $AlN_4$ resonances [264, 268]. The unnarrowed components were largely from mixed nn environments where $C_q$ is thought to be in general larger. MAS NMR spectra where much higher fractions of the aluminium-content narrowed for both 15R and 21R AlN-polytypoid phases showed two distinct Al(4) resonances at 114 and 93 ppm, the latter being assigned to $AlO_3N$ [269]. In conjunction with $^{29}Si$

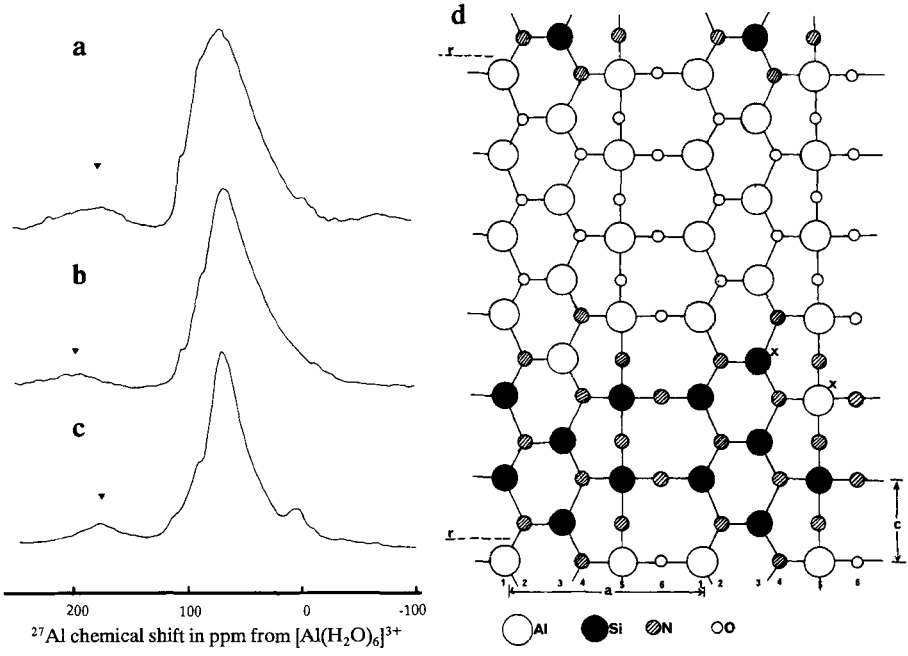


**Fig. 28.** $^{27}$Al MAS NMR spectra at 11.7 T and $\nu_r \sim 15$ kHz for β′- sialons ($Si_{3-x}Al_xO_xN_{4-x}$) for **a** $x = 0.5$, **b** $x = 1$ and **c** $x = 2$ together with **d** a structure consistent with the NMR results.

NMR strict partitioning of oxygen and nitrogen appears to occur so that no Si—O bonds form. The β′-sialon solid solution is formed by isostructural substitution of Al, O for Si, N in β-$Si_3N_4$ to give $Si_{3-x}Al_xO_xN_{4-x}$ ($0 < x < 2$). The $^{29}$Si resonance remains unshifted throughout the composition range at − 48 ppm, corresponding to $SiN_4$ [270]. Early $^{27}$Al MAS NMR spectra were again handicapped by only a small fraction (as little as 10%) being observed and most of that as a broad resonance [73]. There was also a problem with overlapping sidebands obscuring the resonances [73, 271] and TOSS was used to clarify the spectra [272]. However rapid MAS (up to 18 kHz) at 11.7 T produces a more complete and accurate picture of the Al(4) environments present (Fig. 28) [269]. It is clear that $AlN_4$ is a minor environment throughout this series but at low $x$ no $AlO_4$ are present; however these become dominant at high $x$. Hence the different species may be assigned shifts of $AlN_4$ at 108 ppm, $AlO_2N_2$ at 89 ppm and $AlO_3N$ at 75 ppm. This implies a microdomain structure of which a layered form is favoured [73]. Low temperature synthesis of β′-sialon by carbothermal reduction and nitridation of dodecylammonium-exchanged montmorillonite mixed with polyacrylonitrile has been followed by NMR. Thermal decomposition produces initially increasing $AlO_4$ up to 1100°C as a nanocomposite forms which then reacts with nitrogen to form β′-sialon, whose content is maximized at 1300°C. Higher temperatures encourage the formation of SiC

and AlN [273]. Spectra of β″-sialon ($Mg_5AlSi_3O_{11}N$) (67 ppm) [73] and α′-sialon (102 ppm) are dominated by $AlO_4$ and $AlN_4$ respectively.

Incorporation of nitrogen into aluminosilicate glasses has a marked effect on their physical properties. The trivalent nitrogen increases the amount of structural cross-linking which is believed to be the source of increasing viscosity. With 1 wt% nitrogen, glasses showed peaks at 0, 35 and 50 ppm assigned as Al(6), Al(5) and Al(4). Pure aluminosilicate glasses of closely related composition showed no Al(5) [274].

## 15. Conclusion

It has been demonstrated that $^{27}Al$ NMR is of widespread utility in probing many technologically and scientifically important solids at the atomic level. The increased understanding of the influence of the quadrupole interaction on the interpretation of the NMR spectrum and improvements in the experimental technique now allow more complete extraction of $\delta_{iso}$, quadrupole parameters and quantitative information from $^{27}Al$ NMR spectra. Even materials such as $Y_3Al_5O_{12}$ and andalusite that contain aluminium sites with widely differing quadrupole interaction parameters can be accurately quantified. NMR can also probe disordered (both structurally and elementally) materials allowing increased understanding of these materials. One striking example is the obvious widespread occurrence of Al(5) species in glasses and other disordered phases, that NMR has revealed for the first time. It is expected that fast MAS at high applied magnetic fields will increasingly be used as a standard characterization tool of aluminium-containing materials and that the technique will continue to evolve with innovations such as DOR.

## Acknowledgements

I would like to thank Dr. K.R. Carduner who first suggested this project and then provided encouragement in seeing it through and Dr. T.J.M. Bastow for carefully reading and commenting on the manuscript. I would also like to thank Dr. R. Dupree (who also kindly supplied Fig. 15 from his unpublished work) and S.N. Stuart for many useful discussions on NMR and finally all the copyright holders (those stated as the original publishers in the figure captions) who so willingly gave me permission to use figures.

## Appendix

**Table 4.** NMR parameters for aluminium sites in solids.

| Compound | Octahedral | | | Pentahedral | | | Tetrahedral | | | Ref. |
|---|---|---|---|---|---|---|---|---|---|---|
| | $C_q$ (MHz) | $\eta$ | $\delta_{iso}$ (ppm) | $C_q$ (MHz) | $\eta$ | $\delta_{iso}$ (ppm) | $C_q$ (MHz) | $\eta$ | $\delta_{iso}$ (ppm) | |
| $\alpha$-$Al_2O_3$ | 2.39 | 0 | 15 | | | | | | | 66, 275 |
| $\gamma$-$Al_2O_3$ | | | 7.5[1] | | | | | | 66[1] | 3, 6, 84 |
| $\chi$-$Al_2O_3$ | | | 7.5[1] | | | | | | 64[1] | 3, 86 |
| $\varrho$-$Al_2O_3$ | | | 1.9[1] | | | 27[1] | | | 54[1] | 89 |
| Boehmite | | | 3.4[1] | | | | | | | 89 |
| Gibbsite | 2.0 | 0.8 | 11 | | | | | | | 70 |
| | 4.3 | 0.4 | 9 | | | | | | | |
| $Ca_3Al_2O_6 \cdot 6H_2O$ | 0.688 | 0.0 | | | | | | | | |
| $Ca_3Al_2O_6$ | | | | | | | 9.7 | 0.3 | 85 | 101 |
| | | | | | | | 8.69 | 0.32 | 79.5 | 67 |
| | | | | | | | 9.3 | 0.54 | 78 | 67 |
| $Ca_{12}Al_{14}O_{33}$ | | | | | | | 11 | 0.2 | 85 | 101 |
| | | | | | | | 3.7 | 0.9 | 79 | |
| $CaAl_2O_4$ | | | | | | | 2.7 | 0.85 | 83.3 | 101 |
| | | | | | | | | | 80.5 | |
| $Ca_4Al_6O_{13} \cdot 3H_2O$ | | | | | | | 1.8 | 0.5 | 78.2 | 100 |
| $Ca_4Al_6O_{13}$ | | | | | | | 2.4 | 0.95 | 80.3 | 101 |
| $CaAl_4O_7$ | | | | | | | 6.7 | 0.8 | 78 | 101 |
| | | | | | | | 13 | 0.1 | 60[1] | |
| $CaAl_{12}O_{19}$ | 1.5 | 0 | 9 | | | | 2 | 0 | 64[1] | 101 |
| | <1 | 0 | 16 | | | | | | | |
| $KAlO_2 \cdot (1.5H_2O)$ | | | | | | | 5.0 | 0.25 | 81 | 100 |
| $KAlO_2 \cdot H_2O$ | | | | | | | 6.5 | 0.6 | 83 | 100 |
| $KAlO_2 \cdot (0.5H_2O)$ | | | | | | | 5.6 | 0 | 77 | 100 |
| $KAlO_2$ | | | | | | | 1.1 | 0.7 | 76 | 100 |

**Table 4.** (continued)

| Compound | Octahedral | | | Pentahedral | | | Tetrahedral | | | Ref. |
|---|---|---|---|---|---|---|---|---|---|---|
| | $C_q$ (MHz) | $\eta$ | $\delta_{iso}$ (ppm) | $C_q$ (MHz) | $\eta$ | $\delta_{iso}$ (ppm) | $C_q$ (MHz) | $\eta$ | $\delta_{iso}$ (ppm) | |
| $K_2Al_2O(OH)_6$ | | | | | | | 4.46 | 0.2 | 81.3 | 108 |
| $Na_2Al_2O(OH)_6$ | | | | | | | 4.12 | 0.85 | 77 | 108 |
| Dehydrated $Na_2Al_2O(OH)_6$ | | | | | | | 1.9 | n.d. | 81 | 108 |
| β-$NaAlO_2$ | | | | | | | 1.4 | 0.5 | 80.1 | 100 |
| β-$LiAlO_2$ | | | | | | | 1.8 | 0.56 | 82.4 | 10 |
| γ-$LiAlO_2$ | | | | | | | 3.2 | 0.7 | 81.2 | 10 |
| $LiAl_5O_8$ | 4.55 | 0.35 | n.d. | | | | 1.89 | 0[3] | n.d. | 276 |
| $BeAl_2O_4$ | 2.85 | 0.9 | n.d. | | | | | | | 277 |
| $Ba_5Al_2O_8$ | | | | | | | 2.3 | 0.8 | 80 | 100 |
| α-$BaAl_2O_4 \cdot 2H_2O$ | | | | | | | 3.4 | 0.5 | 81 | 100 |
| | | | | | | | 5.1 | 0.9 | 80 | |
| $BaAl_2O_4$ | | | | | | | 2.4 | 0.4 | 78 | 100 |
| $MgAl_2O_4$ | 3.68 | 0 | 7.5[1] | | | | | | 68[1] | 112, 278 |
| $ZnAl_2O_4$ | 3.68 | 0 | n.d. | | | | | | | 279 |
| $YAlO_3$ | 1.3 | 0.2 | 9.4[1] | | | | | | | 73, 280 |
| $LaAlO_3$ | 0.12 | ~0 | 11.7[1] | | | | | | | 101, 281 |
| $Gd_3Al_5O_{12}$ | <0.1 | 0 | | | | | 5.47 | 0 | n.d. | 282 |
| $Y_3Al_5O_{12}$ | 0.63 | 0 | 0.7 | | | | 6.02 | 0 | 78 | 73, 77, 283 |
| $Lu_3Al_5O_{12}$ | 1.15 | 0 | n.d. | | | | 6.4 | 0 | n.d. | 106 |
| $CsAlO_4$ | | | | | | | | | 77[1] | 2 |
| $TlAlO_2$ | | | | | | | | | 69[1] | 100 |
| $CaLaAlO_4$ | 7.0 | | | | | | | | | 105 |
| $CaPrAlO_4$ | 7.5 | | | | | | | | | 105 |
| $CaYAlO_4$ | 7.8 | | | | | | | | | 105 |
| | 9.9 | | | | | | | | | |
| | 12.3 | | | | | | | | | |
| $KAl(SO_4)_2 \cdot 12H_2O$ | 0.4 | 0.0 | −4.1 | | | | | | | 67 |
| $NH_4Al(SO_4)_2 \cdot 12H_2O$ | 0.46 | 0.0 | −0.4 | | | | | | | 67 |
| $Al_2(MoO_4)_3$ | | | 17[1] | | | | | | | 91 |

| | | | | | | | | | | |
|---|---|---|---|---|---|---|---|---|---|---|
| Al dissolved in $TiO_2$ | 2.8 | 1 | −6.5 | | | | | | | 116 |
| $Al_2Ti_2O_5$ | | | 6[1] | | | | | | | 116 |
| $Al_2Ge_2O_7$ | | | | 8.8 | 0.4 | 36 | | | | 26 |
| $LaAlGe_2O_7$ | | | | 7.2 | 0.3 | 35 | | | | 26 |
| $AlNbO_4$ | | | | | | | | | 47[1] | 117 |
| $AlAsO_4$ | | | −1.4[1] | | | | | | | 118 |
| Mordenite | | | | | | | | | 55.8 | 30 |
| Gismondite | | | | | | | | | 56.4 | 30 |
| Na Zeolite A | | | | | | | 1.1 | 0.75 | 59.2 | 30, 40 |
| Analcime | | | | | | | | | 59.4 | 30 |
| Chabazite | | | | | | | | | 59.2 | 30 |
| Gmelinite | | | | | | | | | 59.9 | 30 |
| Microline | | | | | | | 3.22 | 0.21 | 60.9 | 30, 284 |
| Nepheline | | | | | | | | | 61 | 30 |
| | | | | | | | | | 63.5 | |
| Na X,Y zeolite | | | | | | | 2.0 | 0.5 | 62.8 | 30, 285 |
| Hydrated NH4-ZSM-5 | | | | | | | 0.85 | | | 72 |
| Albite | | | | | | | 3.29 | 0.62 | 63 | 30, 284 |
| Natrolite | | | | | | | 1.66 | 0.5 | 64.0 | 30, 285 |
| Sodalite | | | | | | | | | 64.5 | 30 |
| NaCl sodalite | | | | | | | 1.2[2] | | 64.1 | 286 |
| NaBr sodalite | | | | | | | 0.99[2] | | 62.7 | 286 |
| NaI sodalite | | | | | | | 0.77[2] | | 60.7 | 286 |
| Thomosonite | | | | | | | | | 62.7 | 30 |
| | | | | | | | | | 64.4 | |
| | | | | | | | | | 65.8 | |
| Scolecite | | | | | | | | | 62.5 | 30 |
| | | | | | | | | | 66.4 | |
| Pennine | 1.4 | | 10 | | | | 2.8 | | 72.2 | 30 |
| Muscovite | 2.2 | | 5.1 | | | | 2.1 | | 72 | 30 |
| Margarite | 6.3 | | 11 | | | | 4.2 | | 76 | 30 |
| Xantophyllite | 2.0 | | 11 | | | | 2.8 | | 76 | 30 |
| Sillimanite | 8.93 | 0.46 | 64.5 | | | | 6.77 | 0.5 | 4 | 30, 287 |
| Andalusite | 15.6 | 0.08 | 10 | 5.9 | 0.7 | 35 | | | | 30, 59, 6, 2, 63, 288 |

**Table 4.** (continued)

| Compound | Octahedral | | | Pentahedral | | | Tetrahedral | | | Ref. |
|---|---|---|---|---|---|---|---|---|---|---|
| | $C_q$ (MHz) | $\eta$ | $\delta_{iso}$ (ppm) | $C_q$ (MHz) | $\eta$ | $\delta_{iso}$ (ppm) | $C_q$ (MHz) | $\eta$ | $\delta_{iso}$ (ppm) | |
| Kyanite | 10.04 | 0.27 | 15 | | | | | | | 30, 63, |
| | 3.7 | 0.89 | 5 | | | | | | | 289, 290 |
| | 6.53 | 0.59 | 7.5 | | | | | | | |
| | 9.37 | 0.384 | 13 | | | | | | | |
| Cordierite | | | | | | | 10.6 | 0.38 | | 291 |
| | | | | | | | 5.6 | 0.34 | | |
| Zunyite | 2.2 | | 8 | | | | 0.6 | 0 | 72 | 292 |
| Leucite | | | | | | | | | 69.2 | 29 |
| | | | | | | | | | 64.7 | |
| | | | | | | | | | 61.0 | |
| Almadine Garnet | 1.51 | 0 | | | | | | | | 293 |
| Zoisite | 8.05 | 0.46 | | | | | | | | 294 |
| | 18.5 | 0.16 | | | | | | | | |
| Grossular Garnet | 1.6 | 0 | | | | | | | | 295 |
| Epidote | 4.6 | 0.34 | | | | | | | | 150 |
| Vesuvianite | | | 9.0 | | | 41 | | | | 29 |
| | | | 2.5 | | | | | | | |
| Spodumene | 2.95 | 0.94 | | | | | | | | 296 |
| Euclase | 5.17 | 0.7 | | | | | | | | 297 |
| Ephesite | 5.7 | 0.3 | 10.4 | | | | 2.82[2] | | 76.8 | 70 |
| Beryl | 3.09 | 0 | n.d. | | | | | | | 298 |
| Palygorskite | 0.68 | ~1 | 5.5 | | | | | | | 70 |
| Beidellite | | | | | | | 5.6[2] | 0 | 72 | 70 |
| Saponite | | | | | | | 3[2] | | 68 | 70 |
| Montmorillonite | | | | | | | 2.37[2] | | 68.6 | 70 |
| Illite (Interlake) | | | | | | | 3.0[2] | | 72.5 | 70 |
| Rectorite | | | | | | | 2.28[2] | | 72.6 | 70 |
| Cookeite | | | | | | | 3.1[2] | | 74.4 | 70 |
| Vermiculite | | | | | | | 3.9[2] | | 72.0 | 70 |

| | | | | | | | | | | |
|---|---|---|---|---|---|---|---|---|---|---|
| Pyrophyllite | 1.4 | 0 | 4.5 | | | | | | 70 | |
| Pyrophyllite | | | | 10.5 | 0.6 | 29 | | | 180 | |
| Dehydroxylate | | | | | | | | | | |
| Barium aluminium Glycolate | | | | 4 | | 37 | | | 61 | |
| Augelite | 4.5 | 1 | 0.3 | 5.7 | 0.8 | 30.9 | | | 219 | |
| Senegalite | 3.8 | n.d. | 1.7 | 2.6 | n.d. | 36 | | | 219 | |
| Taranakite | | | −3 | | | | | | 220 | |
| $AlPO_4$-21 | | | | 5.1 | 0.4 | 14 | 3.7 | 0.15 | 48 | 62, 229 |
| | | | | 7.4 | 0.65 | 16 | | | | |
| Metavariscite | | | −13.2 | | | | | | | 217 |
| MgAPO-20 | | | | | | | | | 34.4 | 242 |
| $AlPO_4$-25 | | | | | | | 2.3 | 0.67[3] | 39.2 | 229 |
| | | | | | | | 1.1 | 0.67[3] | 37.5 | |
| Hydrated $AlPO_4$-25 | | | | | | | 1.9 | 0.67[3] | 40.8 | 229 |
| | | | | | | | 0.8 | 0.67[3] | 39.5 | |
| Berlinite | | | | | | | 4.09 | 0.37 | 44.8 | 216, 299, 76 |
| T-$AlPO_4$ | | | | | | | 0.75 | 0.95 | 39.8 | 215 |
| C-$AlPO_4$ | | | | | | | 1.2 | 0.75 | 42.5 | 215 |
| $AlPO_4$-5 | | | | | | | 2.3 | 0.95 | 40 | 232 |
| $KAl_2P_4O_{12}$ | 4.9 | 0.37 | −18.2 | | | | | | | 218 |
| *hexagonal*-$AlP_3O_9$ | | | −15.2[1] | | | | | | | 218 |
| tetragonal-$AlP_3O_9$ | | | −20.8[1] | | | | | | | 218 |
| $NH_4AlP_4O_{12}$ | | | −18.7[1] | | | | | | | 218 |
| $NH_4AlHP_3O_{10}$-I | | | −18.7[1] | | | | | | | 218 |
| $NH_4AlHP_3O_{10}$-II | | | −20.7[1] | | | | | | | 218 |
| $KAlHP_3O_{10}$ | | | −13.1[1] | | | | | | | 218 |
| $NH_4AlP_2O_7$ | | | −19.4[1] | | | | | | | 218 |
| $KAlP_2O_7$ | 1.2 | 0.25 | −16.6 | | | | | | | 218 |
| $LiAl(H_2P_2O_7)_2$ | | | −17.3[1] | | | | | | | 218 |
| $KAl(H_2P_2O_7)_2$ | | | −16.6[1] | | | | | | | 218 |
| $Al(H_2PO_4)_3$ | | | −16.6[1] | | | | | | | 218 |
| $NH_4Al_3(H_2PO_4)_6(HPO_4)4H_2O$ | | | −18.7[1] | | | | | | | 218 |
| $Al(H_2O)_3(H_2PO_4)(HPO_4)$ | | | −7.6[1] | | | | | | | 218 |
| Topaz | 1.67 | 0.38 | n.d. | | | | | | | 300 |
| $(NH_4)_3AlF_6$ | | | −0.6[1] | | | | | | | 254 |
| $K_3AlF_6$ | | | −0.1[1] | | | | | | | 254 |

**Table 4.** (continued)

| Compound | Octahedral | | | Pentahedral | | | Tetrahedral | | | Ref. |
|---|---|---|---|---|---|---|---|---|---|---|
| | $C_q$ (MHz) | $\eta$ | $\delta_{iso}$ (ppm) | $C_q$ (MHz) | $\eta$ | $\delta_{iso}$ (ppm) | $C_q$ (MHz) | $\eta$ | $\delta_{iso}$ (ppm) | |
| $H_3AlF_6 \cdot 2H_2O$ | 0.3 | | −2.8[1] | | | | | | | 254 |
| $KH_2AlF_6 \cdot 2H_2O$ | 0.4 | | −2.4[1] | | | | | | | 254 |
| $RbH_2AlF_6 \cdot 2H_2O$ | 0.5 | | −2.7[1] | | | | | | | 254 |
| $(NH_4)_2AlF_5 \cdot H_2O$ | 1.5 | | −2.7[1] | | | | | | | 254 |
| $Rb_2AlF_5 \cdot H_20$ | 3 | | −13.8[1] | | | | | | | 254 |
| $Cs_2AlF_5 \cdot H_2O$ | | | −12[1] | | | | | | | 254 |
| $K_2AlF_5 \cdot H_2O$ | 12 | | | | | | | | | 254 |
| $Rb_2AlF_5 \cdot H_2O$ | 13 | | | | | | | | | 254 |
| $(K,Rb)_2AlF_5 \cdot H_2O$ | 12 | | | | | | | | | 254 |
| $CsAlF_4$ | 12 | | | | | | | | | 254 |
| $NH_4AlF_4$ | 7.5 | | | | | | | | | 254 |
| $KAlF_4$ | 12 | | | | | | | | | 254 |
| $RbAlF_4$ | 13 | | | | | | | | | 254 |
| $RbAlF_4 \cdot 0.5H_2O$ | 13.5 | | | | | | | | | 254 |
| $AlCl_3$ | 0.47 | 0 | n.d. | | | | | | | 301 |
| AlP | | | | | | | ~0 | | 142 | 261 |
| AlAs | | | | | | | ~0 | | 130 | 261 |
| AlSb | | | | | | | ~0 | | 70 | 261 |
| $LiAlH_4$ | | | | | | | 3.9 | 0.3 | 102 | 301 |
| AlN | | | | | | | 2.2 | | 114 | 261 |

[1] Peak position not $\delta_{iso}$.
[2] Second-order quadrupolar effect parameter $C_q(1 + \eta^2/3)^{1/2}$.
[3] Arbitrary choice.
n.d. — not determined.

## References


[1] Andrew E.R.: Int. Rev. Phys. Chem. **1**, 195 (1981)
[2] Muller D., Gessner W., Behrens H.-J., Scheler G.: Chem. Phys. Lett. **79**, 59 (1981)
[3] Mastikhin V.M., Krivoruchko O.P., Zolotovskii B.P., Buyanov R.A.: React. Kinet. Catal. Lett. **1**, 117 (1981)
[4] Fyfe C.A., Thomas J.M., Klinowski J., Gobbi G.C.: Angew. Chem. Int. Ed. Engl. **22**, 259 (1983)
[5] De Jong B.H.W.S., Schramm C.M., Parziale V.E.: Geochim. Cosmochim. Acta **47**, 1223 (1983)
[6] Dupree R., Farnan I.E., Forty A.J., El-Mashri S., Bottyan, L.: J. Phys. Colloq. **C8**, 113 (1985)
[7] Sanz J., Serratosa J.M.: J. Am. Chem. Soc. **106**, 4760 (1984)
[8] Barron P.F., Slade R.C.T., Frost R.L.: J. Phys. Chem. **89**, 3880 (1985)
[9] MacKenzie K.J.D., Brown I.W.M., Meinhold R.H., Bowden M.E.: J. Am. Ceram. Soc. **68**, 293 (1985)
[10] Muller D., Gessner W., Scheler G.: Polyhedron **2**, 1195 (1983)
[11] Cohen M.H., Reif F.: Sol. St. Phys. **5**, 321 (1957)
[12] Volkoff G.M.: Can. J. Phys. **31**, 820 (1953)
[13] Abragam A.: The Principles of Nuclear Magnetism, Chap.6,7. Oxford: Oxford University Press 1983.
[14] Gerstein B.C., Dybowski C.: Transient Techniques in NMR of Solids. New York: Academic Press 1985.
[15] Taulelle F.: NATO ASI Multinuclear Magnetic Resonance in Liquids and Solids – Chemical Applications, p.393. Dordrecht: Kluwer Academic Publishers 1990.
[16] Amoreux J.P., Fernandez C., Granger P.: NATO ASI Magnetic Resonance in Liquids and Solids, p.409. Dordrecht: Kluwer Academic Publishers 1990.
[17] Haeberlen U.: Advances in Magnetic Resonance, Suppl.1. New York: Academic Press 1976.
[18] Maricq M.M., Waugh J.S.: J. Chem. Phys. **70**, 330 (1979)
[19] Kundla.E., Samoson A., Lippmaa E.: Chem. Phys. Lett. **83**, 229 (1981)
[20] Behrens H.J., Schnabel B.: Physica B **114**, 185 (1982)
[21] Muller D.: Ann. Phys. **39**, 451 (1982)
[22] Samoson A., Kundla E., Lippmaa E.: J. Magn. Reson. **49**, 350 (1982)
[23] Samoson A., Lippmaa, E.: Phys. Rev. B **28**, 6567 (1983)
[24] Kundla E.: Proc. Acad. Sci. Estonia SSR **34**, 68 (1985)
[25] Amoureux J.P., Fernandez C., Lefebvre F.: Magn. Reson. Chem. **28**, 5 (1990)
[26] Massiot D., Kahn-Harari A., Michel D., Muller D., Taulelle F.: Magn. Reson. Chem. **28**, S82 (1990)
[27] Samoson A.: Chem. Phys. Lett. **119**, 29 (1985)
[28] Phillips B.L., Kirkpatrick R.J., Putnis A.: Phys. Chem. Minerals **16**, 591 (1989)
[29] Phillips B.L., Allen F.M., Kirkpatrick R.J.: Am. Mineral. **72**, 1190 (1987)
[30] Lippmaa E., Samoson A., Magi M.: J. Am. Chem. Soc. **108**, 1730 (1986)
[31] Ganapathy S., Schramm S., Oldfield E.: J. Chem. Phys. **77**, 4360 (1982)
[32] Kunwar A.C., Thompson A.R., Gutowsky H.S., Oldfield, E.: J. Magn. Reson. **60**, 467 (1894)
[33] Lefebvre F., Amoureux J.P., Fernandez C., Derouane E.: J. Chem. Phys. **60**, 6070 (1987)
[34] Ganapathy G., Shore J., Oldfield E.: Chem. Phys. Lett. **169**, 301 (1990)
[35] Llor A., Virlet J.: Chem. Phys. Lett. **152**, 248 (1988)
[36] Samoson A., Lippmaa E., Pines A.: Mol. Phys. **65**, 1013 (1988)
[37] Mueller K.T., Sun B.Q., Chingas G.C., Zwanziger J.W., Terao T., Pines, A.: J. Magn. Reson. **86**, 470 (1990)
[38] Wu Y., Sun B.Q., Pines A., Samoson A., Lippmaa E.: J. Magn. Reson. **89**, 297 (1990)
[39] Schmidt V.H.: Proc. Ampere Int. Summer School II, p.75, 1971.
[40] Samoson A., Lippmaa E.: Chem. Phys. Lett. **100**, 205 (1983)
[41] Fenzke D., Freude D., Frohlich T., Haase J.: Chem. Phys. Lett. **111**, 171 (1984)

[42] Geurts F.M.M., Kentgens A.P.M., Veeman, W.S.: Chem. Phys. Lett. **120**, 206 (1985)
[43] Man P.P.: J. Magn. Reson. **62**, 78 (1986)
[44] Man P.P., Klinowski J., Trokiner A., Zanni H., Papon P.: Chem. Phys. Lett. **151**, 143 (1988)
[45] Man P.P., Couty R., Fraissard J.: J. Magn. Reson. **86**, 613 (1990)
[46] Kentgens A.P.M., Lemmens J.J.M., Geurts F.M.M., Veeman W.S.: J. Magn. Reson. **71**, 62 (1987)
[47] Samoson A.: Expt. Technik. Phys. **36**, 273 (1988)
[48] Sternheimer R.M.: Phys. Rev. **80**, 102 (1950)
[49] Sternheimer R.M.: Phys. Rev. **95**, 736 (1954)
[50] Schmidt P.C., Sen K.D., Das T.P., Weiss A.: Phys. Rev. B **22**, 4167 (1980)
[51] Bohm J., Fenzke D., Pfeifer H.: J. Magn. Reson. **55**, 197 (1983)
[52] Chu.P.J. Lunsford J.H., Zalewski D.J.: J. Magn. Reson. **46**, 257 (1987)
[53] Hartman J.S., Sherriff B.L.: J. Phys. Chem. **95**, 7575 (1991)
[54] Dec S.F., Wind R.A., Maciel G.E., Anthonio F.E.: J. Magn. Reson. **70**, 355 (1986)
[55] Langer V., Daugaard P., Jakobsen.H.J.: J. Magn. Reson. **70**, 472 (1986)
[56] Jakobsen H.J., Daugaard P., Langer V.: J. Magn. Reson. **76**, 162 (1988)
[57] Wind R.A., Dec S.F., Lock H., Maciel G.E.: J. Magn. Reson. **79**, 136 (1988)
[58] Skibsted J., Bildsoe H., Jakobsen H.J.: J. Magn. Reson. **92**, 669 (1991)
[59] Alemany L.B., Massiot D., Sherriff B.L., Smith M.E., Taulelle F.: Chem. Phys. Lett. **177**, 301 (1991)
[60] Cruikshank M.C., Glasser L.S.D., Barri S.A.I., Poplett I.J.F.: J. Chem. Soc., Chem. Commun. **1986**, 23.
[61] Alemany L.B., Kirker G.W.: J. Am. Chem. Soc. **108**, 6158 (1986)
[62] Alemany L.B., Timken H.K.C., Johnson I.D.: J. Magn. Reson. **80**, 427 (1988)
[63] Dec S.F., Fitzgerald J.J., Frye J.S., Shatlock M.P., Maciel G.E.: J. Magn. Reson. **93**, 403 (1991)
[64] Frye J.S., Maciel G.E.: J. Magn. Reson. **48**, 125 (1982)
[65] Fukushima E., Roeder S.B.W.: Experimental Pulse NMR. Reading: Addison-Wesley 1981.
[66] Jakobsen H.J., Skibsted J., Bildsoe H., Nielsen N.C.: J. Magn. Reson. **85**, 173 (1989)
[67] Skibsted J., Nielsen N.C., Bildsoe H., Jakobsen H.J.: J. Magn. Reson. **95**, 88 (1991)
[68] Nielsen N.C., Bildsoe H., Jakobsen H.J., Norby P.: Zeolites **11**, 622 (1991)
[69] Freude D., Haase J., Klinowski J., Carpenter T.A., Roniker G.: Chem. Phys. Lett. **119**, 365 (1985)
[70] Woessner D.E.: Am. Mineral. **74**, 203 (1989)
[71] Sato R.K., McMillan P.F., Dennison P., Dupree R.: J. Phys. Chem. **95**, 4483 (1991)
[72] Challoner R., Harris R.K.: J. Magn. Reson. **94**, 288 (1991)
[73] Dupree R., Lewis M.H., Smith M.E.: J. Appl. Cryst. **21**, 109 (1988)
[74] Sato R.K., McMillan P.F., Dennison P., Dupree R.: Phys. Chem. Glasses **32**, 149 (1991)
[75] Kirkpatrick R.J., Oestrike R., Weiss C.A., Smith K.A., Oldfield E.: Am. Mineral. **71**, 705 (1986)
[76] Carduner K.R.: J. Magn. Reson. **81**, 312 (1989)
[77] Massiot D., Bessada C., Coutures J.P., Taulelle F.: J. Magn. Reson. **90**, 231 (1990)
[78] Haase J., Pfeifer H., Oehme W., Klinowski J.: J. Chem. Soc., Chem. Commun. **1988**, 1142.
[79] Andrew E.R., Tunstall D.P.: Proc. Phys. Soc. **78**, 1 (1961)
[80] Woessner D.E., Timken H.K.C.: J. Magn. Reson. **90**, 411 (1990)
[81] Morris H.D., Ellis P.D.: J. Am. Chem. Soc. **111**, 6045 (1989)
[82] Morris H.D., Bank S., Ellis P.D.: J. Phys. Chem. **94**, 6045 (1990)
[83] Kellberg L., Linsten M., Jakobsen H.J.: Chem. Phys. Lett. **182**, 120 (1991)
[84] Rocha J., Klinowski J.: J. Chem. Soc., Chem. Commun. **1991**, 1121.
[85] Kohn S.C., Dupree R., Mortuza M.G., Henderson C.M.B.: Am. Mineral. **76**, 309 (1991)
[86] John C.S., Alma N.C.M., Hays G.R.: Appl. Catal. **6**, 341 (1983)
[87] Krivoruchko O.P., Mastikhin V.M., Zolotovskii B.P., Paramzin S.M., Klevtsov D.P., Buyanov R.A.: Kinet. Catal. **5**, 664 (1985)

[88] Paramzin S.M., Zolotovskii B.P., Krivoruchko O.P., Buyanov, R.A. in: Proceedings 6th Int. Symp. Heterogeneous Catal., Part 2, p.169, Sofia, Bulgaria 1987.
[89] Slade R.C.T., Southern J.C., Thompson I.M.: J. Mater. Chem. **1**, 563 (1991)
[90] Pearson R.M., Schramm C.M.: Colloids and Surfaces **45**, 323 (1990)
[91] McMillan M., Brinen J.S., Haller G.L.: J. Catal. **97**, 243 (1986)
[92] Fitzgerald J.J.: Anitiperspirants and Deodorants, p.119. New York: Marcel Dekker 1988.
[93] Komarneni S., Roy R., Fyfe C.A., Kennedy G.J.: J. Am. Ceram. Soc. **68**, C243 (1985)
[94] Olsen W.L., Bauer L.J.: Mater. Res. Soc. Symp. Proc. **73**, 189 (1986)
[95] Covino J., Nissan R.A.: Mater. Res. Soc. Symp. Proc. **73**, 565 (1986)
[96] Nortier P., Fourre P., Mohammed-Saad A.B., Saur O., Lovel J.C.: Appl. Catal. **61**, 141 (1990)
[97] Nishio T., Fujiki Y.: J. Ceram. Soc. Japan Int. Ed. **98**, 1232 (1990)
[98] Farnan I., Dupree R., Forty A.J., Jeong Y.S., Thompson G.E., Wood G.C.: Phil. Mag. Lett. **59**, 189 (1989)
[99] Engelhardt G., Michel D.: High Resolution Solid State NMR of Silicates and Zeolites. Chichester: John Wiley and Sons 1987.
[100] Muller D., Gessner W., Samoson A., Lippmaa E., Scheler G.: J. Chem. Soc. Dalton Trans. **1986**, 1277.
[101] Muller D., Gessner W., Samoson A., Lippmaa E., Scheler G.: Polyhedron **5**, 779 (1986)
[102] Gessner W., Muller D., Behrens H.J., Scheler G.: Z. Anorg. Allg. Chem. **486**, 193 (1982)
[103] Gessner W., Muller D., Schubert H.: Z. Anorg. Allg. Chem. **529**, 56 (1985)
[104] Dupree R., Lewis M.H., Smith M.E.: J. Am. Chem. Soc. **111**, 5125 (1989)
[105] Vorotilova L.S., Dmitriova L.V.: Sov. Phys. Crystall. **34**, 623 (1989)
[106] Efitsenko P.Y., Hazanov E.N., Ivanov S.N., Medved V.V., Tcharnaya E.V.: Phys. Lett. A **147**, 135 (1990)
[107] Massiot D., Taulelle F., Coutures J.P.: J. Phys. Colloq. **51**, C5-425 (1990)
[108] Dec S.F., Maciel G.E., Fitzgerald J.J.: J. Am. Chem. Soc. **112**, 9069 (1990)
[109] Gobbi G.C., Christoffersen R., Otten M.T., Miner B., Buseck P.R., Kennedy G.J., Fyfe C.A.: Chem. Lett. **1985**, 771.
[110] Wood B.J., Kirkpatrick R.J., Montez B.: Am. Mineral. **77**, 999 (1986)
[111] Dupree R., Lewis M.H., Smith M.E.: Phil. Mag. A **53**, L17 (1986)
[112] Ibarra A., Vila R., Jimenez de Castro M.: Phil. Mag. Lett. **65**, 45 (1991)
[113] Muller D., Rettel A., Gessner W., Scheler G.: J. Magn. Reson. **57**, 152 (1984)
[114] Rettel A., Gessner W., Muller D., Scheler G.: Brit. Ceram. Trans. J. **84**, 25 (1985)
[115] Luong T., Mayer H., Eckert H., Novinson T.I.: J. Am. Ceram. Soc. **72**, 2136 (1989)
[116] Stebbins J.F., Farnan I., Klabunde U.: J. Am. Ceram. Soc. **72**, 2198 (1989)
[117] Pries de Oliveira P.G., Lefebvre F., Eon J.G., Volta J.C.: J. Chem. Soc., Chem. Commun. **1990** 1480.
[118] Chen J., Xu R., Xu Y., Qiu J.: J. Chem. Soc. Dalton Trans. **1990**, 3319.
[119] Klinowski J.: Prog. NMR Spec. **16**, 237 (1984)
[120] Klinowski J.: Colloids and Surfaces **36**, 133 (1989)
[121] Fyfe C.A., Kokotailo G.T., Gies H., Strobl H. in: Multinuclear Magnetic Resonance in Liquids and Solids – Chemical Applications, p.425. Dordrecht: Kluwer Academic Publishers 1990.
[122] Vega A.J., Luz Z.: J. Phys. Chem. **91**, 365 (1987)
[123] Luz Z, Vega A.J.: J. Phys. Chem. **91**, 374 (1987)
[124] Haase J., Pfeifer H., Oehme W., Klinowski J.: Chem. Phys. Lett. **150**, 189 (1988)
[125] Klinowski J., Thomas, J.M., Fyfe C.A., Gobbi G.C.: Nature **296**, 533 (1982)
[126] Scholle K.F.M.G.J., Veeman W.S.: J. Phys. Chem. **89**, 1850 (1985)
[127] Fyfe C.A., Gobbi G.C., Kennedy G.J., Graham J.D., Ozubko R.S., Murphy W.J., Bothnerby A., Pudok J., Chesnick A.S.: Zeolites **5**, 179 (1985)
[128] Klinowski J., Anderson M.W.: J. Chem. Soc. Faraday Trans. I **82**, 569 (1986)
[129] Massiani P., Fajula F., Di Renzo F.: J. Chem. Soc., Chem. Commun. **1988**, 814.

[130] Massiani P., Chauvin B., Fajula F., Figeueras F., Guegeun G.: Appl. Catal. **42**, 105 (1988)
[131] Freude D., Haase J., Pfeifer H., Prager D., Scheler, G.: Chem. Phys. Lett. **114**, 143 (1985)
[132] Corbin D.R., Farlee R.D., Stucky G.D.: Inorg. Chem. **23**, 2920 (1984)
[133] Bosacek V., Mastikhin V.M.: J. Phys. Chem. **91**, 260 (1987)
[134] Freude D., Brunner E., Pfeifer H., Prager D., Jerschkewitz H.-G., Lohse U., Oehlmann G.: Chem. Phys. Lett. **139**, 325 (1987)
[135] Samoson A., Lippmaa E., Engelhardt G., Lohse G., Jerschkewitz H.-G.: Chem. Phys. Lett. **139**, 325 (1987)
[136] Hamdan H., Klinowski J.: Chem. Phys. Lett. **158**, 447 (1989)
[137] Klinowski J., Fyfe C.A., Gobbi G.C.: J. Chem. Soc. Faraday Trans. I **81**, 3003 (1985)
[138] Sanz J., Fornes V., Corma A.: J. Chem. Soc. Faraday Trans I **84**, 3113 (1988)
[139] Cruz J.M., Corma A., Fornes V.: Appl. Catal. **50**, 287 (1989)
[140] Ray G.J., Meyer B.L., Marshall G.L.: Zeolites **7**, 307 (1987)
[141] Sulikowski B., Borbely G., Beyer H.K., Karge H.G., Mishin I.W.: J. Phys. Chem. **93**, 3240 (1989)
[142] Hey M.J., Nock A., Rudham R., Appleyard I.P., Haines G.A.J., Harris R.K.: J. Chem. Soc. Faraday Trans. I **82**, 2817 (1986)
[143] Grobet P.J., Jacobs P.A., Beyer H.K.: Zeolites **6**, 47 (1986)
[144] Klinowski J., Thomas J.M., Fyfe C.A., Gobbi G.C., Hartman J.S.: Inorg. Chem. **22**, 63 (1983)
[145] Corbin D.R., Burgess B.F., Vega A.J., Farlee R.D.: Anal. Chem. **59**, 2722 (1987)
[146] Grobet P.J., Geerts H., Martens J.A., Jacobs P.A.: J. Chem. Soc., Chem. Commun. **1987** 1688.
[147] Gilson J.P., Edwards G.C., Peters A.W., Rajogopalan K., Wormshocker R.F., Roberie T.G., Shatlock M.P.: J. Chem. Soc., Chem. Commun. **1987** 91.
[148] Kirkpatrick R.J.: Rev. Mineral. **18**, 341 (1988)
[149] Kirkpatrick R.J., Phillips B.L.: Appl. Magn. Reson. **4** (1993) (this issue)
[150] Ghose S., Tsang T.: Am. Mineral. **58**,748 (1973)
[151] Merwin L.H., Sebald A., Rager H., Schneider H.: Phys. Chem. Minerals **18**, 47 (1991)
[152] Sanz J., Sobrados J., Cavalieri A.L., Pena P., Aza S., Moya J.S.: J. Am. Ceram. Soc. **74**, 2398 (1991)
[153] Kirkpatrick R.J., Kinsey R.A., Smith K.A., Henderson D.M. , Oldfield E.: Am. Mineral. **70**, 106 (1985)
[154] Phillips B.L., Kirkpatrick R.J., Hovis G.L.: Phys. Chem. Minerals **16**, 262 (1988)
[155] Yang W.H., Kirkpatrick R.J., Henderson D.M.: Am. Mineral. **71**, 712 (1988)
[156] Sherriff B.L., Grundy H.D., Hartmann J.S.: Can. Mineral. **25**, 717 (1987)
[157] McMillan P., Akaogi M., Ohtani E., Williams E., Niemann R., Sato R.: Phys. Chem. Minerals **16**, 428 (1989)
[158] Kinsey R.A., Kirkpatrick R.J., Hower J., Smith K.A., Oldfield.E.: Am. Mineral. **70**, 537 (1985)
[159] Thompson J.G.: Clay Minerals **19**, 229 (1984)
[160] Komarneni S., Fyfe C.A., Kennedy G.J.: Clay Minerals **20**, 327 (1985)
[161] Komarneni S., Fyfe C.A., Kennedy G.J., Strobl H.: J. Am. Ceram. Soc. **69**, C45 (1986)
[162] Alma N.C.M., Hays G.R., Samoson A., Lippmaa E.T.: Anal. Chem. **56**, 729 (1984)
[163] Komarneni S., Roy R., Roy D.M., Fyfe C.A., Kennedy G.J., Bothnerby A.A., Dadok J., Chesnik A.S.: J. Mater. Sci. **20**, 4209 (1985)
[164] Goodman B.A., Russel J.D., Montez B., Oldfield E., Kirkpatrick R.J.: Phys. Chem. Minerals **12**, 342 (1985)
[165] Wada K., Wilson M., Kakuto Y., Wada S.I. Clays and Clay Minerals **36**, 11 (1988)
[166] Wilson M.A., McCarthy S.A., Fredricks P.M.: Clay Minerals **21**, 879 (1986)
[167] Wada K., Kakuto Y., Wilson M.A., Hanna, J.V.: Clay Minerals **26**, 449 (1991)
[168] Jakobsen H.J., Jacobsen H., Lindgreen H.: Fuel **67**, 727 (1985)
[169] Komarneni S., Tsuji M.: J. Am. Ceram. Soc. **72**, 1668 (1989)
[170] Brown I.W.M., MacKenzie K.J.D., Bowden M.E., Meinhold R.H.: J. Am. Ceram. Soc. **68**, 298 (1985)

[171] Watanabe I., Shimzu H., Nagasawa K., Masuda A., Saito H.: Clay Minerals **22**, 37 (1987)
[172] Sanz J., Madani A., Serratosa J.M., Moya J.S., Aza S.: J. Am. Ceram. Soc. **71**, C418 (1988)
[173] Lambert J.F., Millman W.S., Fripiat J.J.: J. Am. Chem. Soc. **111**, 3517 (1989)
[174] Fitzgerald J.J., Hamza A.I., Bronnimann C.E., Dec S.F.: Solid State Ionics **32/33**, 378 (1989)
[175] Rocha J., Klinowski J.: Phys. Chem. Minerals **17**, 179 (1990)
[176] Slade R.C.T., Davies T.W.: J. Mater. Chem. **1**, 361 (1991)
[177] Rocha J., Klinowski J.: J. Chem. Soc., Chem. Commun. **1991**, 582.
[178] Kodama H., Kotlyar L.S., Ripmeester J.A.: Clays and Clay Minerals **37**, 364 (1989)
[179] Wilson M.A., Young B.C., Scott K.M.: Fuel **65**, 1584 (1986)
[180] Fitzgerald J.J., Dec S.F., Hamza A.I.: Am. Mineral. **74**, 1405 (1989)
[181] Frost R.L., Barron P.F.: J. Phys. Chem. **88**, 6206 (1984)
[182] Brown I.W.M., MacKenzie K.J.D., Meinhold R.H.: J. Mater. Sci. **22**, 3265 (1987)
[183] MacKenzie K.J.D., Brown I.W.M., Cardile C.M., Meinhold R.H.: J. Mater. Sci. **22**, 2645 (1987)
[184] Mackenzie K.J.D., Bowden M.E., Brown I.W.M., Meinhold R.H.: Clays and Clay Minerals **37**, 317 (1989)
[185] Wilson M.A., Wada K., Wada S.I., Kakuto Y.: Clay Minerals **23**, 175 (1988)
[186] Komarneni S.: Clays and Clay Minerals **37**, 469 (1989)
[187] Mandair A.-P.S., McWhinnie W.R.: Polyhedron **14**, 1709 (1990)
[188] Tennakoon D.T.B., Thomas J.M., Jones W., Carpenter T.A., Ramdas S.: J. Chem. Soc. Faraday Trans. I **82**, 545 (1986)
[189] Tennakoon D.T.B., Jones W., Thomas J.M., Ballantine J.H., Purnell J.H.: Solid State Ionics **24**, 205 (1987)
[190] Anderson M.W., Klinowski J.: Inorg. Chem. **29**, 3260 (1990)
[191] Risbud S.H., Kirkpatrick R.J., Taglialavore A.P., Montez B.: J. Am. Ceram. Soc. **70**, C10 (1987)
[192] Yasumori A., Iwasaki M., Kawazoe H., Yamari M., Nakamura Y.: Phys. Chem. Glasses **31** 1 (1990)
[193] Engelhardt G., Nofz M., Forkel K., Wilsmann.I.G., Magi M., Samoson A., Lippmaa E.: Phys. Chem. Glasses **26**, 157 (1985)
[194] Dupree R., Holland D., Williams D.S.: J. Phys. Colloq. **46**, C8-119 (1985)
[195] Oestrike R., Yang W.H., Kirkpatrick R.J., Hervig R.L., Navrotsky A., Montez B.: Geochim. Cosmoschim. Acta **51**, 2199 (1987)
[196] Merzbacher C.I., Sherriff B.L., Hartman J.S., White W.B.: J. Non-Cryst. Solids **124**, 194 (1990)
[197] Hamilton D.L., Chesworth W., Kennedy G., Fyfe C.A.: Geochim. Cosmoschim. Acta **50**, 123 (1986)
[198] Hallas E., Hahnert M.: Z. Chem. **26**, 188 (1986)
[199] Ohtani E., Taulelle F., Angell C.A.: Nature **314**, 78 (1985)
[200] Stebbins J.F., Sykes.D.: Am. Mineral. **75** 943 (1990)
[201] Yang W.H.A., Kirkpatrick R.J.: Geochim. Cosmoschim. Acta **53**, 805 (1989)
[202] Yang W.H.A., Kirkpatrick R.J.: Am. Mineral. **75**, 1009 (1990)
[203] Kohn S.C., Dupree R., Smith M.E.: Geochim. Cosmoschim. Acta **53**, 2925 (1989)
[204] Mandair A.-P.S., McWhinnie W.R.: Polyhedron **10**, 55 (1991)
[205] Thomas J.M., Klinowski J., Wright P.A., Roy R.: Angew. Chem. Int. Ed. **22**, 614 (1983)
[206] Couty R., Taulelle F., Theveneau H.: C.R. Acad. Sc. Paris II **301**, 14 (1985)
[207] Komarneni S., Roy R, Fyfe C.A., Kennedy G.J., Strobl H.: J. Am. Ceram. Soc. **69**, C43 (1986)
[208] Couty R., Taulelle F., Theveneau H.: C.R. Acad. Sc. Paris II **302**, 1005 (1986)
[209] Couty R., Taulelle F., Zanni-Theveneau H.: C.R. Acad. Sc. Paris II **304**, 165 (1987)
[210] Pouxviel J.C., Boilot J.P., Poncelet G., Hubert-Pfalz L.G., Lecombe A., Dauger A., Beloeil J.C.: J. Non-Cryst. Solids **93**, 177 (1987)
[211] Irwin A.D., Holmgren J.S., Jonas J.S.: J. Mater. Sci. **23**, 2980 (1988)
[212] Selvaraj U., Komarneni S., Roy R.: J. Am. Ceram. Soc. **73**, 3663 (1990)

[213] Engelhardt G., Fahlke B., Magi M., Lippmaa E.: Zeolites **5**, 49 (1985)
[214] Hietato S.L., Smith D.M., Brinker C.J., Hurd A.J., Carim A.H., Dando N.: J. Am. Ceram. Soc. **73**, 2815 (1990)
[215] Marra R.A., Dando N.R. in: Symp. High Temp. Comp., Proc. Am. Soc. Comp., p.158, 1989.
[216] Muller D., Jahn E., Ladwig G., Haubenreisser U.: Chem. Phys. Lett. **109**, 332 (1984)
[217] Blackwell C.S., Patton R.L.: J. Phys. Chem. **88**, 6135 (1984)
[218] Muller D., Grunze I., Hallas E., Ladwig G.: Z. Anorg. Allg. Chem. **500**, 80 (1988)
[219] Bleam W.F., Dec S.F., Frye J.S.: Phys. Chem. Minerals **16**, 817 (1989)
[220] Bleam W.F., Pfeffer P.E., Frye J.S.: Phys. Chem. Minerals **16**, 809 (1989)
[221] Dollase W.A., Merwin L.H., Sebald A.: J. Sol. St. Chem. **83**, 140 (1989)
[222] Meinhold R.H., Tapp N.V.: J. Chem. Soc., Chem. Commun. **1990**, 219.
[223] Meinhold R.H., Tapp N.V.: Zeolites **11**, 401 (1990)
[224] Rocha J., Liu X., Klinowski J.: Chem. Phys. Lett. **182**, 531 (1991)
[225] Tapp N.V., Milestone N.B., Bowden M.E., Meinhold R.H.: Zeolites **10**, 151 (1990)
[226] Jahn E., Muller D., Becker K.: Zeolites **10**, 151 (1990)
[227] Barrie P.J., Smith M.E., Klinowski J.: Chem. Phys. Lett. **180**, 6 (1991)
[228] Blackwell C.S., Patton R.L.: J. Phys. Chem. **92**, 3965 (1988)
[229] Jelinek R., Chmelka B.F., Wu Y., Grandinetti P.J., Pines A., Barrie P.J., Klinowski J.: J. Am. Chem. Soc. **113**, 4097 (1991)
[230] Wu Y., Chmelka B.F., Pines A.Davis, M.E., Grobet P.J., Jacobs P.A.: Nature **346**, 550 (1990)
[231] Grobet P.J., Martens J.A., Balakrishnan I., Martens M., Jacobs P.A.: Appl. Catal. **56**, L21 (1989)
[232] Muller D., Jahn E., Fahlke B., Ladwig G., Haubenreisser U.: Zeolites **5**, 53 (1985)
[233] Jahn E., Muller D., Wieker W., Richter-Mendau J.: Zeolites **9**, 177 (1989)
[234] Cheung T.P.P., Willcox K.W., McDaniel M.P., Johnson M.M., Bronnimann C., Frye.J.: J. Catal. **102**, 10 (1986)
[235] Hasha D., Saldarraj L.S., Saldarraj C., Hathaway P.E., Cox D.F., Davis M.E.: J. Am. Chem. Soc. **110**, 2127 (1988)
[236] Freude D., Ernst H., Hunger M., Pfeifer H., Jahn E.: Chem. Phys. Lett. **143**, 477 (1983)
[237] Appleyard I.P., Harris R.K., Fitch F.R.: Chem. Lett. **1985**, 1747.
[238] Derouane E.G., Maistraiu L., Gabelica Z., Tuel.A., Nagy J.B., Ballmoos R.V.: Appl. Catal. **51**, L13 (1989)
[239] Jahn E., Muller D., Becker K.: Zeolites **10**, 151 (1990)
[240] Maistraiu L., Dumont N., Nagy J.B., Gabelica Z., Derouane E.G.: Zeolites **10**, 243 (1989)
[241] Appleyard I.P., Harris R.K., Fitch F.R.: Zeolites **6**, 428 (1986)
[242] Barrie P.J., Klinowski J.: J. Phys. Chem. **93**, 5972 (1989)
[243] Goldfarb D.: Zeolites **9**, 509 (1989)
[244] Muller D., Berger G., Grunze I., Ladwig G., Hallas E., Haubenreisser U.: Phys. Chem. Glasses **24**, 37 (1983)
[245] Brow R.K., Kirkpatrick R.J., Turner G.L.: J. Am. Ceram. Soc. **73**, 2293 (1990)
[246] Haubenreisser U., Hallas E., Cuttmacher K.H., Schnabel B., Schreder T.: Proc. Symp. Modern Methods on RF Spec., p.215, 1981.
[247] Dupree R., Holland D., Mortuza M.G., Collins J.A., Lockyer.M.W.G.: J. Non-Cryst. Solids **112**, 111 (1989)
[248] Hahnert M., Hallas E.: Rev. Chim. Minerale **24**, 221 (1987)
[249] Hallas E., Hahnert M.: Cryst. Res. Technol. **20**, K25 (1985)
[250] Dupree R., Holland D., Williams D.S.: Phys. Chem. Glasses **26**, 50 (1958)
[251] Bunker B.C., Kirkpatrick R.J., Brow R.K., Turner G.L., Nelson C.: J. Am. Ceram. Soc. **74**, 1430 (1991)
[252] Hallas E., Gerth K., Hahnert M.: Z. Chem. **27**, 270 (1987)
[253] Oestrike R., Navrotsky A., Turner G.L., Montez B., Kirkpatrick R.J.: Am. Mineral. **72**, 788 (1987)
[254] Muller D., Bentzig U.: Z. Anorg. Allg. Chem. **17**, 525 (1989)

[255] Fletcher J.B., Risbud S.H., Hayashi S., Kirkpatrick R.J.: Diffusion Defect Data **53**, 493 (1987)
[256] Shelby J.E., Shaw C.M., Spess M.S.: J. Appl. Phys. **66**, 1149 (1989)
[257] Shelby J.E., Lord C.E.: J. Am. Ceram. Soc. **73**, 750 (1990)
[258] Groat L.A., Raudsepp M., Hawthorne F.C., Ercit T.S., Sherriff B.L., Hartman J.S.: Am. Mineral. **75**, 992 (1990)
[259] Andrew E.R., Hinshaw W.S., Tiffen R.S.: Phys. Lett. **46A** 57 (1973)
[260] Rubini S., Dimitropoulos C., Gotthardth R., Borsa F.: Phys. Rev. B **44**, 2019 (1991)
[261] Han O.H., Timken H.Y.C., Oldfield E.: J. Chem. Phys. **89**, 6046 (1988)
[262] Sears R.E.J.: Phys. Rev. B **22**, 1135 (1980)
[263] Akimoto K., Mori Y., Kojima G.: Phys. Rev. B **35**, 3799 (1987)
[264] Butler N.D., Dupree R., Lewis M.H.: J. Mater. Sci. Lett. **3**, 469 (1984)
[265] Marshall G.L., Harris R.K., Apperley D., Yeung R.: Proc. Symp. Sci. Ceram. **14**, 347 (1987)
[266] Haase J., Freude D., Frohlich T., Himpel G., Kerber F., Lippmaa E., Pfeifer H., Sarv P., Schafer H., Sieffert B.: Chem. Phys. Lett. **156**, 328 (1989)
[267] Hayashi S., Hayamizu K., Yamaoto O.: Bull. Chem. Soc. Japan **60**, 761 (1987)
[268] Klinowski J., Thomas J.M., Thompson D.P., Korgul P., Jack K.H., Fyfe, C.A., Gobbi G.C.: Polyhedron **3**, 1267 (1984)
[269] Smith.M.E.: J. Phys. Chem. **96** 1444 (1992)
[270] Dupree R., Lewis M.H., Leng-Ward G., Williams D.S.: J. Mater. Sci. Lett. **4**, 393 (1985)
[271] Sato R.K., MacMillan P.F. in: Conference Proceedings Industry/University Advanced Materials Symp., p.759. Advanced Materials Institute Golden Co. 1989.
[272] Carduner K.R., Carter R.O., Rokosz M.J., Peters C., Crosbie G.M., Stiles E.D.: Chem. Mater. **1**, 302 (1989)
[273] Bastow T., Hardin S.G., Turney T.W.: J. Mater. Sci. **26**, 1443 (1991)
[274] Sato R.K., Bolvin J., McMillan P.F.: J. Am. Ceram. Soc. **73**, 2494 (1990)
[275] Pound R.V.: Phys. Rev. **79**, 685 (1950)
[276] Stauss G.K.: J. Chem. Phys. **40**, 1988 (1964)
[277] Hockenberry J.H., Brown L.C., Williams D.: J. Chem. Phys. **28**, 367 (1958)
[278] Brun E., Hafner S.S.: Z. Kristall. **117**, 37 (1962)
[279] Brun E., Ghose S., Schindler P.: Helv. Phys. Acta **37**, 626 (1964)
[280] Gorchulski T., Zbieranowski W.: Magnetic Resonance, Related Phenomena. p.973, 1979.
[281] Muller K.A., Brun E., Derighetti B., Drumheller J.G., Waldner F.: Phys. Lett. **9**, 223 (1964)
[282] Euler F., Bruce J.A.: Acta Crystal. **19**, 971 (1965)
[283] Brog K.C., Jones W.H., Verker C.M.: Phys. Lett. **20**, 258 (1966)
[284] Hafner S.S., Hartmann P.: Helv. Phys. Acta **37**, 348 (1964)
[285] Petch H.E.N., Pennington K.S.: J. Chem. Phys. **36**, 1216 (1962)
[286] Jacobsen H.S., Norby P., Bildsoe H., Jakobsen H.J.: Zeolites **9**, 491 (1989)
[287] Raymond M., Hafner S.S.: J. Chem. Phys. **53**, 4110 (1970)
[288] Hafner S.S., Raymond M., Ghose S.: J. Chem. Phys. **52**, 6037 (1970)
[289] Hafner S.S., Raymond M.: Am. Mineral. **52**, 1632 (1967)
[290] Lee D., Bray P.J.: J. Magn. Reson. **94**, 51 (1991)
[291] Tsang T., Ghose S.: J. Chem. Phys. **56**, 3329 (1972)
[292] Kunwar A.C., Thompson A.R., Gutowsky H.S., Oldfield E.: J. Magn. Reson. **60**, 467 (1980)
[293] Ghose S.: Solid State Commun. **2**, 361 (1964)
[294] Brinkmann D., Staehli D.J.L., Ghose S.: J. Chem. Phys. **51**, 5128 (1969)
[295] Derighetti B., Ghose S.: Phys. Lett. **28A**, 523 (1969)
[296] Petch H.E., Cranna N.G., Volkoff G.M.: Can. J. Phys. **31**, 837 (1953)
[297] Eades R.G.: Can. J. Phys. **33**, 286 (1955)
[298] Brun E., Hartmann P., Laves F., Schwartzenbach D.: Helv. Phys. Acta **34**, 388 (1961)
[299] Brown L.C., Williams D.: J. Chem. Phys. **24**, 751 (1956).
[300] Tsang T., Ghose S.: J. Chem. Phys. **56**, 261 (1972)

[301] Casabella P.A., Miller N.C.: J. Chem. Phys. **40**, 1362 (1964)
[302] Kellberg L., Bildsoe H., Jakobsen H.J.: J. Chem. Soc., Chem. Commun. **1990**, 1294

**Author's address:** Dr. Mark E. Smith, Department of Physics, University of Kent, Canterbury, Kent, CT2 7NZ, England